Optical Ranging: Synchronous-Mode Concept, Prototype, and Validation

Marc Sanchez Net*

ABSTRACT. — This article describes a synchronous ranging system to estimate the range between a spacecraft and a ground station from an optical uplink and downlink. Time transfer between the uplink and downlink is achieved by (1) synchronizing the uplink and downlink symbol clocks at the spacecraft, and (2) defining a new protocol data unit, termed *ranging codeword*, to provide sufficient range ambiguity resolution.

The article is divided into three parts. First, it explains the general concept of a synchronous ranging system, including how range estimates can be recovered from phase measurements and how the system operates when used in conjunction with the protocol stack defined by the Consultative Committee for Space Data Systems for high photon efficiency optical links. Secondly, this article derives the necessary equations to estimate the system performance assuming that both the spacecraft and ground station use a photon-counting device to receive the optical system.

Finally, the third part of this article describes a software prototype developed at the Jet Propulsion Laboratory to validate the operation of a synchronous ranging system. To do so, I utilize channel conditions representative of the Deep Space Optical Communications experiment on board the Psyche spacecraft and showcase the achievable ranging performance in two scenarios, one with benign channel conditions and one with expected channel conditions at 1 AU.

I. Introduction

Optical ranging is a generic term used to denote the set of technologies required to estimate the distance between a spacecraft and a reference point, nominally a ground

*Communications Architectures and Research Section.

The research described in this publication was carried out by the Jet Propulsion Laboratory, California Institute of Technology, under a contract with the National Aeronautics and Space Administration.

station on Earth.[1] Currently, the Consultative Committee for Space Data Systems (CCSDS) is considering standardizing two alternative methods to achieve optical ranging, henceforth termed *synchronous* and *asynchronous modes*.

A previous article described the principle of operation of the asynchronous mode [1], which is based on the already standardized Radio Frequency (RF) Telemetry Ranging [2]. Here, we instead focus our attention on the synchronous mode and describe (1) its principle of operation and (2) the prototyping effort undertaken at the Jet Propulsion Laboratory (JPL) to validate its operation and demonstrate its capabilities. Note that this prototyping effort also serves as one of the (at least) two implementations required by CCSDS prior to issuing a new standard.

The synchronous mode of operation is based on the Time-of-Flight experiment performed by the Lunar Laser Communication Demonstration (LLCD) on board the Lunar Atmosphere and Dust Environment Explorer (LADEE) [3]. In particular, this experiment demonstrated centimeter-level ranging capability using an optical uplink and downlink from the Moon, albeit after several post-processing steps to eliminate several artifacts induced by technical limitations of the flight and ground terminals, which were not specifically designed for ranging purposes.

A. The CCSDS Protocol Stack

To understand the principle of operation of the synchronous mode, a basic understanding of the protocol stack as defined by the CCSDS is necessary, particularly the optical communications standards currently available for High Photon Efficiency (HPE) systems [4, 5].

The primary concern of HPE systems is power efficiency. Consequently, information is modulated onto the optical channel using Pulse-Position Modulation (PPM). In PPM, each channel symbol comprises M time slots, followed by P guard slots (see Figure 1). One of the M time slots contains signal photons, depending on the symbol being transmitted (e.g., see blue slot in Figure 1), while all other $M-1$ slots only contain background noise photons. Similarly, the P guard slots never contain signal photons and are used at the transmitter to accommodate physical laser requirements and at the receiver to aid in slot synchronization.

CCSDS has standardized two HPE signaling schemes, known as HPE telemetry and HPE beacon, and optional accompanying data signaling [5]. In HPE telemetry, a PPM symbol can have order M equal to $\{4, 8, 16, 32, 64, 128, 256\}$, the number of guard slots is equal to $P = M/4$, and the slot duration $T_s = \{\,0.125,\ 0.25,\ 0.5,\ 1,\ 2,\ 4,\ 8,\ 16,\ 32,\ 64,\ 128,\ 256,\ 512\,\}$ ns. This, together with the other parameters of the standard, allow the link to operate at information rates as high as 2.1 Gbps and as low as 485 bps, approximately. On the other hand, the HPE beacon-plus-accompanying-data format is

[1] Optical ranging via a relay is beyond the scope of this article.

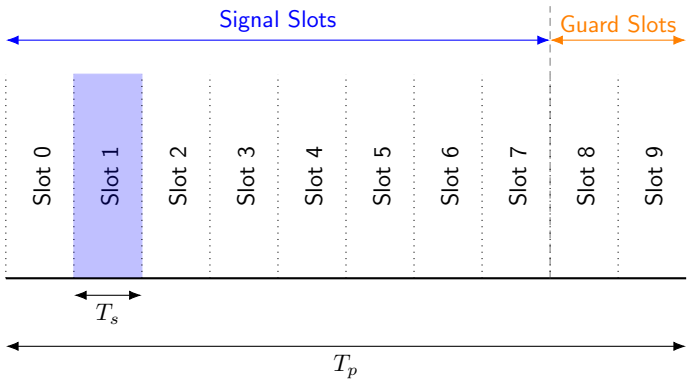

Figure 1. Symbol Structure for an M-PPM Modulation with $M/4$ Guard Slots with $M = 8$.

more constrained and only admits $M = 2$, $P = 2$, and a slot width of $T_s = 65536$ ns, resulting in information rates ranging from 2 kbps to 18 bps, approximately.

To generate the stream of PPM symbols to be transmitted over the optical channel, the CCSDS optical standard defines several protocol data units (PDUs) and processing steps to transform a set of logical binary information bits into a collection of PPM symbols and guard slots. These steps include, among others, randomization, encoding, interleaving, and addition of synchronization markers [5]. A detailed description of these steps is not necessary for this article. However, because the synchronous mode of operations relies on synchronization markers to generate the necessary ranging observables, a basic understanding of the PDUs transmitted over the channel is now provided. In particular, several PDUs are defined as follows:

- A *codeword* is a set of PPM symbols available at the output of the encoder. Each codeword is generated by taking as input k information bits; adding $n - k$ redundancy bits, possibly interleaving them; and outputting $n/\log_2 M$ M-ary symbols, where k/n is known as the code rate.[2]
- An *interleaved codeword* (ICW) is generated by taking as input one or multiple codewords, processing their PPM symbols via an interleaver, and grouping the resulting symbols in chunks of length $n/\log_2 M$.
- A *synchronization-marked codeword*[3] (SMCW) is obtained by concatenating a codeword synchronization marker[4] (CSM) and an ICW. The sequence of PPM

[2]Note that this description implicitly assumes the use of a block code of rate k/n.

[3]Different CCSDS standards have different names for an SMCW. For example, the CCSDS Telecommand standard calls it a Communications Links Transmission Unit (CLTU), while the Telemetry standard calls it a Channel Access Data Unit (CADU). Currently, the CCSDS HPE optical standards do not have a specific name for it.

[4]Different CCSDS standards have different names from the synchronization marker. Furthermore, markers might be placed between multiple codewords, rather than once per codeword.

symbols that define a CSM is provided in [5] and depends on the signaling format.

- A repeated SMCW is generated by taking an ICW and repeating each M-ary PPM symbol Q times to form a super-symbol. This increases the available signal power at the receiver at the expense of information rate.

This protocol structure is depicted in Figure 2. Note that each PPM symbol is represented here by a number ranging from 0 to $M-1$, which indicates the time slot in the symbol that is activated.

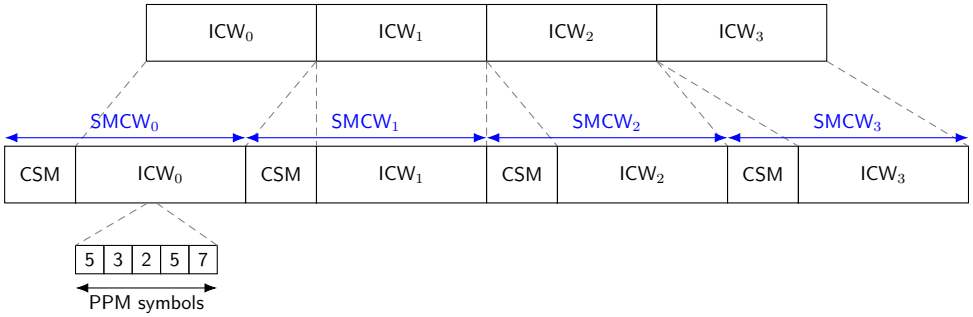

Figure 2. SMCW Structure Assuming 8-PPM Symbols and No Repetition.

For the proposed synchronous ranging, an additional protocol data unit must be defined, which is termed a *ranging codeword* here (RCW). An RCW contains $N \geq 1$ contiguous SMCWs and is delimited by a special synchronization marker called a *range synchronization marker* (RSM), a structure shown in Figure 3. Note, however, that in the special case where $N = 1$, an RCW is equivalent to an SMCW and, consequently, the RCW is delimited by the CSM instead of being replaced by the RSM.

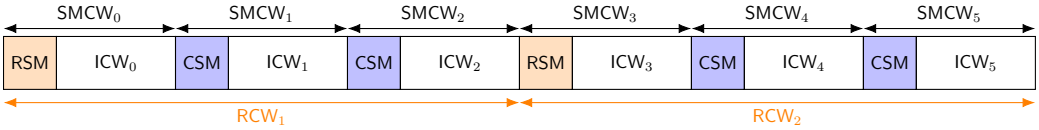

Figure 3. RSM Structure with $N = 3$ SMCW per RCW.

B. PPM Signal Model and Phase Definition

Consider an optical PPM signal being sent by a transmitter. It can be expressed mathematically as

$$x(t) = \sum_{m=-\infty}^{\infty} \sum_{q=0}^{Q-1} p(t - i_m T_s + (q + mQ)T), \tag{1}$$

where $T = (M + P)T_s$ denotes the duration of a PPM symbol, plus its guard slots; $p(t)$ is a rectangular pulse of duration T_s; M and P denote the number of signal slots and guard slots per PPM symbol; Q is the repeat factor; and $\{i_m\}$ is a sequence of independent and identically distributed uniform random numbers taking values $\{0, 1, ..., M - 1\}$.

Define the phase of the transmitted signal as a real number that indicates the possibly partial number of PPM symbols that have elapsed since the start of transmission. In other words,

$$\psi_T(t) = Qm(t) + q(t) + i(t), \tag{2}$$

where $m(t)$ and $q(t)$ are integers such that

$$m(t) = \left\lfloor \frac{t}{QT} \right\rfloor \tag{3}$$

$$q(t) = \left\lfloor \frac{t}{T} - m(t)Q \right\rfloor, \tag{4}$$

and i is a fractional number between zero and one:

$$i(t) = t - (m(t)Q + q(t))T. \tag{5}$$

Here, $m(t)$ counts the integer number of Q-repeated PPM symbols plus guard time completely transmitted by time t; $q(t)$ denotes the integer number of PPM symbols plus guard time completely sent in the current Q-repeated symbol; and $i(t)$ is a real number between 0 and 1 that indicates the part of the current PPM symbol that has been transmitted. Note that, as defined, $\psi_T(t)$ is an unwrapped phase. In other words, it grows from zero to infinity.

The signal arrives at the receiver after a certain propagation delay, which is in general time varying and denoted by $\tau(t)$. Therefore, it can be expressed mathematically as

$$r(t) = \sum_{m=-\infty}^{\infty} \sum_{q=0}^{Q-1} p(t - \tau(t) - i_m T_s + (q + mQ)T). \tag{6}$$

The phase of the received signal, denoted by $\psi_R(t)$, is again a fractional number that counts, at a given time t, the number of PPM symbols that have elapsed since the start of transmission. It is constructed in a similar manner as $\psi_T(t)$, albeit in this case the explicit expressions have to account for the fact that, at reception, the duration of a PPM symbol plus guard time may no longer equal to T.

Additionally, it is also convenient to define the *relative* phase of the received signal with respect to the transmitted signal as

$$\varphi(t) = \frac{\tau(t)}{T}. \tag{7}$$

This phase can be decomposed in two parts, an integral and a fractional part:

$$\varphi_s(t) = \left\lfloor \frac{\tau(t)}{T} \right\rfloor \tag{8}$$

$$\varphi_f(t) = \frac{\tau(t)}{T} - \varphi_s(t). \tag{9}$$

The phase estimator at the receiver tracks a wrapped version of $\varphi_f(t)$ and provides the generated estimates to a Phase-Locked Loop (PLL) that filters out part of the noise and recovers an unwrapped version of $\varphi_f(t)$. Therefore, in this article we will assume that the relative phase measured at the receiver is directly equal to the unwrapped version of $\varphi_f(t)$. Furthermore, we will denote it by $\varphi(t)$ to simplify the notation.

C. One-Way and Two-Way Propagation Delay

This section introduces several concepts and notations that are useful when studying a two-way synchronous ranging. In particular, let $d(t)$ be a time-varying function that specifies the relative distance between a ground station and a spacecraft, and assume that the optical signal propagates at the speed of light c so that the propagation delay is simply

$$\tau(t) = \frac{d(t)}{c}. \tag{10}$$

Then this article defines the following quantities:

- $\tau_u(t)$ denotes the uplink one-way propagation delay experienced by a signal departing at time t from a known reference point in the ground station.
- $\tau_d(t)$ denotes the downlink one-way propagation delay experienced by a signal departing at time t from a known reference point in the spacecraft.
- $\tau_{ud}(t)$ denotes the uplink-plus-downlink propagation delay, also known as round-trip light-time (RTLT) delay, experienced by a signal departing at time t from a known reference point in the ground station.
- $\tilde{\tau}_u(t)$ denotes the uplink one-way propagation delay experienced by a signal arriving at time t to a known reference point in the spacecraft.
- $\tilde{\tau}_d(t)$ denotes the downlink one-way propagation delay experienced by a signal arriving at time t to a known reference in the ground station.
- $\tilde{\tau}_{ud}(t)$ denotes the uplink-plus-downlink propagation delay experienced by a signal arriving at time t from a known reference point in the ground station.

Figure 4 shows the difference between $\tau(t)$ and $\tilde{\tau}(t)$ assuming that $d(t)$ is a linear function. Observe that with the exception of the trivial and unrealistic case where $d(t)$

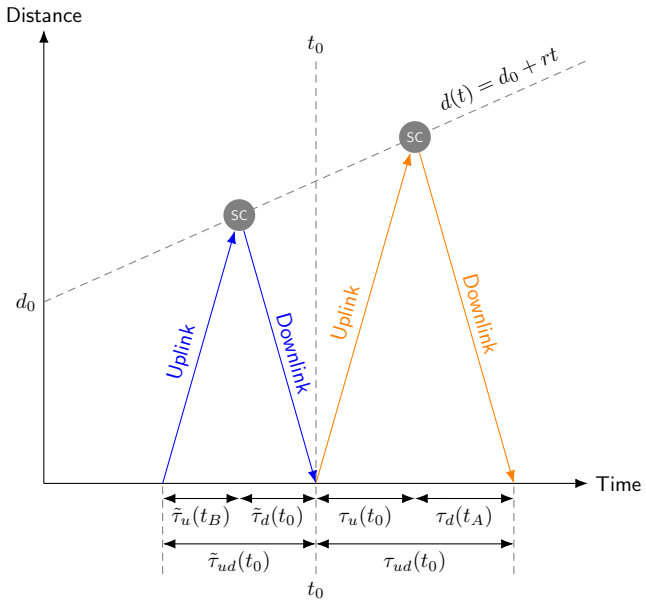

Figure 4. Forward and Backward Round-trip Light-Time Delays. In the figure, $t_A = t_0 + \tau_u(t_0)$ and $t_B = t_0 - \tilde{\tau}_d(t_0)$. "SC" denotes spacecraft.

is constant, we have that $\tau_u(t) \neq \tilde{\tau}_u(t)$, $\tau_d(t) \neq \tilde{\tau}_d(t)$, and $\tau_{ud}(t) \neq \tilde{\tau}_{ud}(t)$. However, the following relationships do hold:

$$\tau_{ud}(t) = \tau_u(t) + \tau_d(t + \tau_u(t)) + \tau_{sc} \tag{11}$$

$$\tilde{\tau}_{ud}(t) = \tilde{\tau}_u(t - \tilde{\tau}_d(t)) + \tilde{\tau}_d(t) + \tau_{sc}, \tag{12}$$

where τ_{sc} denotes the delay experienced onboard the spacecraft as the signal travels from a known reference point on the receiver to a known reference point on the transmitter (Figure 4 assumes $\tau_{sc} = 0$ for simplicity's sake).

Furthermore, it is sometimes advantageous to explicitly differentiate between the times of departure and arrival of the signal. Therefore, this article defines the following notation:

- t_T denotes the time of departure from the ground station.
- t_S denotes the time of arrival to the spacecraft. Unless stated otherwise, assume $\tau_{sc} = 0$ so that t_S is also equal to the time of departure from the spacecraft.
- t_R denotes the time of arrival to the ground station.

Note the following relationships in the "forward" time direction:

$$t_S = t_T + \tau_u(t_T) \tag{13}$$

$$t_R = t_S + \tau_d(t_S) = t_T + \tau_{ud}(t_T), \tag{14}$$

and the following relationships in the "backward" time direction:

$$t_S = t_R - \tilde{\tau}_d(t_R) \tag{15}$$

$$t_T = t_S - \tilde{\tau}_u(t_S) = t_R - \tilde{\tau}_{ud}(t_R), \tag{16}$$

which result in

$$\tau_{ud}(t_T) = \tilde{\tau}_{ud}(t_R). \tag{17}$$

II. Principle of Operation

A synchronous ranging system measures the range between a spacecraft and a ground station by synchronizing the phase of the received uplink and transmitted downlink RCWs (hence the name "synchronous mode"). Once clock synchronization is achieved, the spacecraft transponder acts as a time transfer mechanism in which the start of transmission of a downlink RCW occurs a fixed duration after the arrival of an RCW on the uplink.

To illustrate the principle of operation of the synchronous ranging mode, this section is divided into three parts. First, it describes a synchronous ranging system under idealized conditions, which helps clarify the key conditions that must be met for successful operation of the system. Next, this section discusses the effect of several nonideal factors that must be taken into account in a technically implementable synchronous ranging system. This includes, for example, the need to calibrate delays between electronic subsystems at the ground station and onboard the spacecraft, as well as the effect of spacecraft dynamics on the ranging system. Finally, this section concludes by describing how the synchronous ranging system operates when the spacecraft moves with respect to the tracking ground station.

A. Idealized Ranging System

Consider an idealized synchronous ranging system that operates in an environment such that the relative distance between the spacecraft and ground station is constant. The structure of the system is shown in Figure 5, assuming that

- one uplink RCW is equal to $N_u = 1$ SMCW;
- one downlink RCW is equal to $N_d = 5$ SMCWs[5];
- the departure of downlink RCW (denoted by $\mathrm{RCW_d}$) starts exactly when an uplink RCW arrives (denoted by $\mathrm{RCW_u}$), as highlighted by the blue dotted lines;
- the range rate between the spacecraft and the ground station is zero;
- there are no signal delays at the ground station or the spacecraft;

[5] $N_d = 5$ is chosen here arbitrarily for the sake of clarity.

- and all electromagnetic signals travel at the speed of light c.

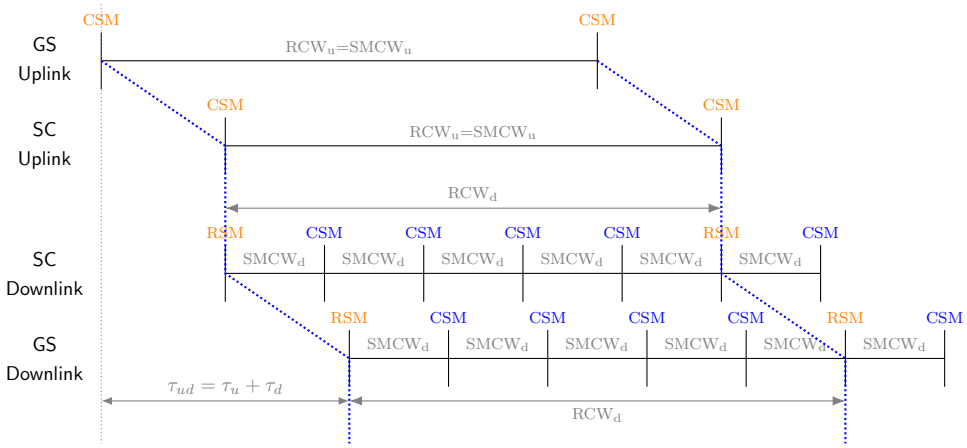

Figure 5. Idealized Synchronous Ranging System. "GS" denotes a ground station.

The phase measured by this ranging system is relative to the start of an RCW. Furthermore, the system is constructed so that the duration of a downlink RCW equals the duration of an uplink RCW, measured *at the spacecraft*.[6] This ensures that the arrival of an RCW on the uplink is time-aligned with the departure of an RCW on the downlink.

To guarantee that the system achieves synchronicity and maintains it over time, two conditions must be met: First, the spacecraft radio must synchronize the uplink and downlink slot and symbol clocks. Second, the number of SMCWs per uplink RCW must be integrally related to the number of SMCWs per downlink RCW. This can be observed in Figure 5, which arbitrarily uses an integral relationship of 1:5 for demonstration purposes.

To illustrate how a range measurement is recovered in this idealized ranging system, consider the system in Figure 6 and assume that a range measurement for the spacecraft is to be obtained at time t_R. At that time, the ground station measures two quantities, the phase of the transmitted signal $\psi_T(t_R)$ and the phase of the received signal $\psi_R(t_R)$, which are both measured from the leading edge of an RSM (or the leading edge of a CSM if $N = 1$). Furthermore, if $\psi_T(t_T)$ was known, then

$$\psi_T(t_R) = \frac{t_R}{T_u} = \frac{t_T + \tau_{ud}(t_T)}{T_u} \tag{18}$$

$$\psi_T(t_T) = \frac{t_T}{T_u}, \tag{19}$$

where T_u denotes the duration of an uplink PPM symbol (and we have implicitly

[6] This distinction is important because in a system with range dynamics (i.e., the distance between the spacecraft and the ground station varies over time), the duration of SMCW$_u$ when it departs the ground station is different than when it arrives at the spacecraft.

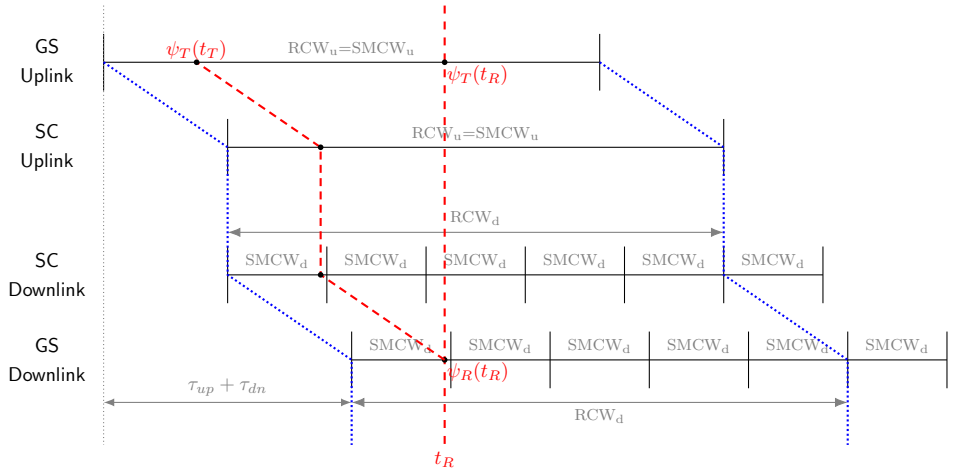

Figure 6. Idealized Range Measurement.

assumed that transmission started at $t = 0$). Consequently,

$$\psi_T(t_R) - \psi_T(t_T) = \frac{\tau_{ud}(t_T)}{T_u} \tag{20}$$

from which the RTLT and distance could be directly inferred. Note that, using this procedure, the system would either estimate $\tau_{ud}(t_T)$ or $\tilde{\tau}_{ud}(t_R)$, and thus care must be exercised to associate the measurement with the appropriate instant of time.

At the ground station, ψ_T can be recorded over time and stored for post-processing. However, $\psi_T(t_T)$ is not directly known because t_T is unknown. But thanks to the restrictions imposed in the synchronous ranging system, the phase measured on the downlink $\psi_R(t_R)$ is equal to a scaled version of the phase transmitted one RTLT ago. Namely,

$$\psi_R(t_R)\beta = \psi_T(t_R - \tilde{\tau}_{ud}(t_R)) = \psi_T(t_T), \tag{21}$$

where $\beta = \frac{T_d}{T_u}$ is a conversion factor that relates the duration of a downlink and uplink PPM symbol, plus their guard times. Therefore, after substituting Equation (21) into Equation (20) and solving for the RTLT, we get

$$\tau_{ud}(t_T) = T_u\psi_T(t_R) - T_d\psi_R(t_R). \tag{22}$$

Furthermore, because we have assumed that (1) the spacecraft and ground station are stationary with respect to each other and (2) all electromagnetic signals travel at the speed of light, we know that

$$\tau_{ud}(t) = \frac{2d(t)}{c}. \tag{23}$$

Therefore, combining Equations (22) and (23) results in

$$d(t_T) = \frac{c}{2}\left[T_u\psi_T(t_R) - T_d\psi_R(t_R)\right]. \tag{24}$$

Finally, note that in a practical system, $\psi_T(t_R)$ might not be available if the RTLT delay is very long (e.g., it takes several hours for a signal sent from Earth to reach the Voyager spacecraft). In that case, $\tau_{ud}(t)$ can still be measured as long as the departure time t_T can be recovered from $\beta\psi_R(t_R)$.

B. Calibration Delays

The analysis developed in Section II.A assumes several idealized conditions not realizable in real life. This section succinctly addresses one of them, namely the calibration delays that need to be measured and subtracted prior to range measurement estimate. Note that this is not the main purpose of this article, so the treatment offered here is rather superficial. Instead, see [2] and [6] for a more in-depth treatment of the different delays that must be calibrated.

First, consider the problem of delays introduced by the ground station measurement system. Traditionally, ranging measurements at the Deep Space Network (DSN) have been obtained with respect to the antenna used for ranging purposes, more specifically the intersection of the azimuth and elevation axes of the parabolic reflector. This point of reference is chosen because its position on Earth is known (and can be propagated) with a high degree of precision, thus providing an accurately known point of reference for navigation purposes.

However, the electronic equipment in charge of recording the uplink and downlink phases is not located at the antenna but rather at the signal-processing center (SPC), possibly a few kilometers away from the parabolic reflector. Therefore, when estimating τ_{ud}, it is necessary to subtract the delay introduced by the ground lines connecting the SPC and the antenna. In other words, under the assumption of an ideal spacecraft transponder, the distance estimate between the ground antenna and the spacecraft is computed as

$$d(t_R) = \frac{c}{2}\left[\tau_{ud} - \tau_{up}^{gs} - \tau_{dn}^{gs}\right], \tag{25}$$

where τ_{up}^{gs} is the propagation delay between the SPC's uplink electronics and the DSN antenna, and τ_{dn}^{gs} is the same quantity measured between the antenna and the SPC's downlink electronics. Note that τ_{up}^{gs} and τ_{dn}^{gs} are not necessarily constant over long timescales, so the DSN performs periodic calibration exercises to ensure that their magnitudes are well characterized.

Next, consider the ability of the spacecraft to perfectly synchronize the uplink and downlink RCWs. Two effects must be considered: synchronization errors induced by noise and residual delays introduced by the spacecraft electronics. The former cannot be calibrated away due to their stochastic nature but rather impose a lower limit on the system's range resolution. Estimating the range error induced by noise is typically performed during mission planning using a ranging link budget and ensures that the available ranging techniques are sufficient to meet the mission ranging requirements.

Alternatively, residual delays introduced by the spacecraft electronics are typically calibrated while testing the spacecraft's transponder prior to launch and then subtracted from the range estimate.[7] In other words, the range estimate will now be obtained as

$$d(t_R) = \frac{c}{2}\left[\tau_{ud} - \tau_{up}^{gs} - \tau_{dn}^{gs} - \tau_{sc}\right], \tag{26}$$

where τ_{sc} is the propagation delay between the two spacecraft reference points, one on the uplink and one on the downlink (for spacecraft with a single antenna used in full duplex mode, a single reference point may be used). Note that, from a practical standpoint, this effect prevents the spacecraft radio from transmitting a downlink RCW exactly at the same time that an uplink RCW starts arriving (as shown in Figures 5 and 6). Instead, the downlink RCW will depart a certain delay after the arrival of each uplink RCW, but what really matters is for this delay to remain constant.

C. Spacecraft Dynamics

This section considers how spacecraft dynamics affect the synchronous ranging system presented in this section. In general, these spacecraft dynamics are caused by the relative motion between the spacecraft and the ground telescope making the ranging measurement—more precisely, the radial component of the spacecraft's velocity.

To model this effect, let us assume that the distance between the spacecraft and the ground station is variable over time and denote it by $d(t)$. Furthermore, for a reasonably short period of time (e.g., a few hours), and assuming no impulsive maneuvers or planetary entries are performed during the ranging period, this function can be approximated as linear:

$$d(t) = d_0 + r \cdot t, \tag{27}$$

where d_0 denotes the distance at the beginning of the ranging track, and r denotes the range rate, in units of distance per second. Note that under certain circumstances (e.g., propulsive maneuver, orbital insertion) higher-order terms should also be included (e.g., range acceleration), but they are neglected here for simplicity's sake.

The range rate essentially introduces two effects on a narrowband signal: First, it modifies the received carrier frequency, i.e., the well-known Doppler effect; and second, it modifies the duration of the received slots and symbols. For the purposes of this article, assume that perfect Doppler pre-compensation at the ground station is performed both on the transmit and receive side, so the Doppler effect can be ignored. Alternatively, the effect of the range rate on the symbol and slot duration must be

[7] Ranging systems require these delays to be as deterministic as possible for calibration purposes. Therefore, system implementation is done using programmable hardware components, such as FPGAs, for which the time delay in a given signal path is measurable during the synthesis process.

properly characterized and accounted for when simulating and validating the synchronous ranging mode.

To better understand this effect, consider the "time deformation" experienced by one of the slots transmitted by the ground station under the linear range assumption (see Figure 7). In particular, it is shown in Appendix II that, at the spacecraft, this same slot will last

$$T_s^{sc} = \frac{1}{1-\gamma} T_s \approx (1+\gamma) T_s \tag{28}$$

with $\gamma = \frac{r}{c}$. Similarly, if the spacecraft uplink and downlink are synchronous, then the slot arriving to the ground station via the downlink will last

$$T_s^{gs} = \frac{1+\gamma}{1-\gamma} T_s \approx (1+2\gamma) T_s. \tag{29}$$

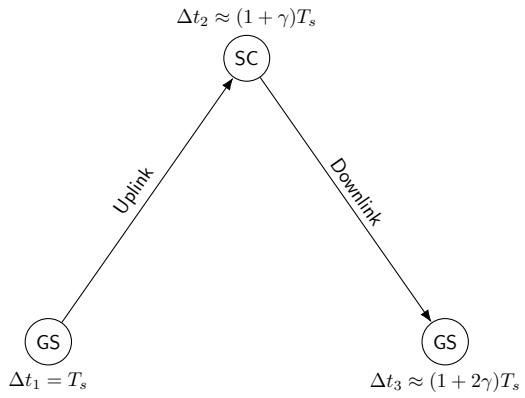

Figure 7. Stretching of the Duration of a PDU Due to Range Rate.

Note that this analysis is not unique to a slot. In fact, any PDU lasting T seconds when departing the ground station will last approximately $(1+\gamma)T$ seconds when it arrives to the spacecraft. Note also that the sign of γ dictates whether the PDU duration increases or decreases. Indeed, if the spacecraft is going away from Earth, then γ is positive, and thus the PDU "stretches" in time. In contrast, when the spacecraft is headed towards Earth, $\gamma < 0$ and thus the PDU "shrinks."[8]

D. Range Measurement with Spacecraft Dynamics

Now, consider the issue of recovering a range measurement from phase observables obtained from a synchronous ranging system in the presence of spacecraft dynamics. In this case, we know that Equation (23) will not hold in general and, consequently,

[8] One might argue that the explanation presented here is just a rewording of the Doppler effect. However, this article avoids the term "Doppler effect" because it deals solely with a noncoherent modulation in which the carrier frequency is not tracked in any way.

the ranging problem has two parts: First, use a radiometric system to estimate $\tau_{ud}(t)$; and second, use trajectory and gravitational models to derive $d(t)$ from the observed values of the $\tau_{ud}(t)$.

Let us first consider the problem of estimating $\tau_{ud}(t)$. As indicated in [2], the ranging system estimates the RTLT delay from the following equation

$$\int_{t_T}^{t_R} \dot{\psi}_T(t)dt = \psi_T(t_R) - \psi_T(t_T), \tag{30}$$

where $\dot{\psi}_T(t)$ denotes the derivative of the phase of the transmitted signal by the ground station, which can be easily recorded by its uplink subsystem. Note that Equation (30) is just the fundamental theorem of calculus applied to the transmitted phase $\psi_T(t)$. Furthermore, thanks to the restrictions imposed by the synchronous ranging system, we know that

$$\psi_R(t_R)\beta = \psi_T(t_T). \tag{31}$$

Therefore, we can solve Equation (30) by replacing the unknown quantity $\psi_T(t_T)$ by the measurable quantity $\psi_R(t_R)\beta$ and solving the resulting equation for t_T. For example, assume that the ground station transmits an uplink optical signal where the PPM symbols have constant duration. Then,

$$\dot{\psi}_T(t) = \frac{d}{dt}\frac{t}{T_u} = \frac{1}{T_u} \tag{32}$$

and equation (30) simplifies to

$$\frac{t_R - t_T}{T_u} = \psi_T(t_R) - \psi_R(t_R)\beta. \tag{33}$$

Consequently, we can obtain an estimate of the RTLT delay as

$$\tau_{ud}(t_T) = T_u\psi_T(t_R) - T_d\psi_R(t_R) = \tilde{\tau}_{ud}(t_R). \tag{34}$$

Next, we need to recover a range estimate from $\tau_{ud}(t)$. To do so, Appendix III shows that for a linear spacecraft trajectory

$$\tau_{ud}(t_T) = \frac{1}{1-\gamma}\frac{2d(t_T)}{c} + (1+\gamma)\tau_{sc} \tag{35}$$

$$\tilde{\tau}_{ud}(t_R) = \frac{1}{1+\gamma}\frac{2d(t_R)}{c} + (1-\gamma)\tau_{sc}. \tag{36}$$

Therefore,

$$d(t_T) = \frac{c}{2}\left[(\tau_{ud}(t_T) - \tau_{sc}) - \gamma\left(\tau_{ud}(t_T) + \tau_{sc}\right)\right] \tag{37}$$

$$d(t_R) = \frac{c}{2}\left[(\tilde{\tau}_{ud}(t_R) - \tau_{sc}) + \gamma\left(\tilde{\tau}_{ud}(t_R) + \tau_{sc}\right)\right]. \tag{38}$$

E. Range Synchronization Marker

So far, this article has described the operation of a synchronous ranging system using RCWs that are delimited by a special type of synchronization marker, which is called an RSM. However, this article has not specified the RSM value, nor how they relate to the normal CSMs already specified in the CCSDS HPE standards.

The fundamental property of a synchronization marker is that it should be easily identifiable using a correlator. Therefore, they are typically designed so that their autocorrelation function exhibits a large peak at zero lag and a reasonably low value at any other lag. Formally, let a synchronization marker be defined as a sequence s of S PPM symbols taking values $0, 1, ..., M-1$. Then the autocorrelation function for a lag l is defined as

$$R[l] = \sum_{i=1}^{S} I\left(s[i], s[i+l]\right), \tag{39}$$

where $I(a, b)$ is an indicator function such that

$$I(a,b) = \begin{cases} 1 & a = b \\ 0 & a \neq b. \end{cases} \tag{40}$$

Note that with this definition, $R[0] = S$. Furthermore, to find a "good" synchronization marker, the following figure of metric must be minimized:

$$\xi_1 = \max_{l \neq 0} R[l]. \tag{41}$$

To design the RSM, however, another metric needs to be optimized. Namely, the cross-correlation between the RSM and the CSM must be low so that the receiver can easily differentiate between the two types of synchronization markers. To formalize this concept, let s_{rsm} denote the sequence of PPM symbols of the RSM and assume that it has length S_{csm}. Then, its cross-correlation with the CSM is defined as

$$X_{csm}^{rsm}[l] = \sum_{i=1}^{S_{csm}} I\left(s_{rsm}[i], s_{csm}[i+l]\right). \tag{42}$$

Therefore, to design the RSM, we must solve a multi-objective optimization problem in which both ξ_1 and ξ_2 are minimized, with

$$\xi_2 = \max_{l} X_{csm}^{rsm}[l]. \tag{43}$$

To solve this problem, two options are possible. For short synchronization markers and low M, full factorial enumeration over all possible synchronization sequences can be performed. Each candidate RSM sequence is then evaluated against ξ_1 and ξ_2 and

the best candidate is selected.[9] For problems in which full factorial enumeration is computationally intractable, I utilized a multi-objective Genetic Algorithm (MOGA) that converges towards a set of Pareto-optimal RSMs. This MOGA was configured to evaluate 1000 populations with 1000 candidate RSMs per population.

The results of this optimization process are provided in Figure 8, which provides a comparison of the CSM and RSM autocorrelation as well as the cross-correlation between the CSM and RSM.[10] Observe that the RSM sequences obtained by the MOGA exhibit an autocorrelation that is at least as good as the CSM, if not better. Similarly, the cross-correlation between the RSM and the CSM is typically as low as the autocorrelation of the CSM for $l \neq 0$, except for a couple cases where it is slightly higher but well within acceptable operational limits.

III. Performance of a Synchronous Ranging System

This section describes the theoretical performance of an optical synchronous ranging system. In particular, it studies the performance of the tracking loops on the spacecraft and ground station receivers, which ultimately determine the accuracy with which the uplink and downlink phases can be measured.

A. System Model

To model the system, assume that both the spacecraft and the ground station receiver use a one-shot phase estimator plus a PLL to track the phase of the received signal. This is representative, for example, of the way the phase is tracked in operational optical receivers developed by JPL [7].

In Figure 9, $\varphi_u(t)$ is the phase of the uplink signal as it arrives to the spacecraft.[11] This phase is first estimated by a one-shot estimator $\hat{\varphi}_u^{os}(t')$, and its output is provided to a PLL that filters out noise and thus generates an improved estimate, which we denote by $\hat{\varphi}_u(t')$. This PLL is assumed to be of second-order, and its coefficients are calculated from the desired normalized loop bandwidth and the update rate of the PLL according to the equations in [8]. However, higher-order PLLs can also be modeled at the expense of increased computational complexity.

Note that in Figure 9, two time indices, t and t', are used. They emphasize the fact that for the system to operate, there is no need for the spacecraft to have a clock that

---

[9] As with any multi-objective optimization problem, there is no single "best" solution that minimizes all figures of merit. Instead, the solution is a Pareto front, i.e., a set of solutions in which a metric cannot be improved without worsening another one. Therefore, to select a final solution, it is up to the user to express the relative preference between the figures of merit. For our purposes, I pick RSM sequences that roughly assign equal weight to ξ_1 and ξ_2.

[10] The RSM sequences are provided in Appendix I.

[11] Recall here that $\varphi(t)$ denotes a relative phase, as described in Section I.B.

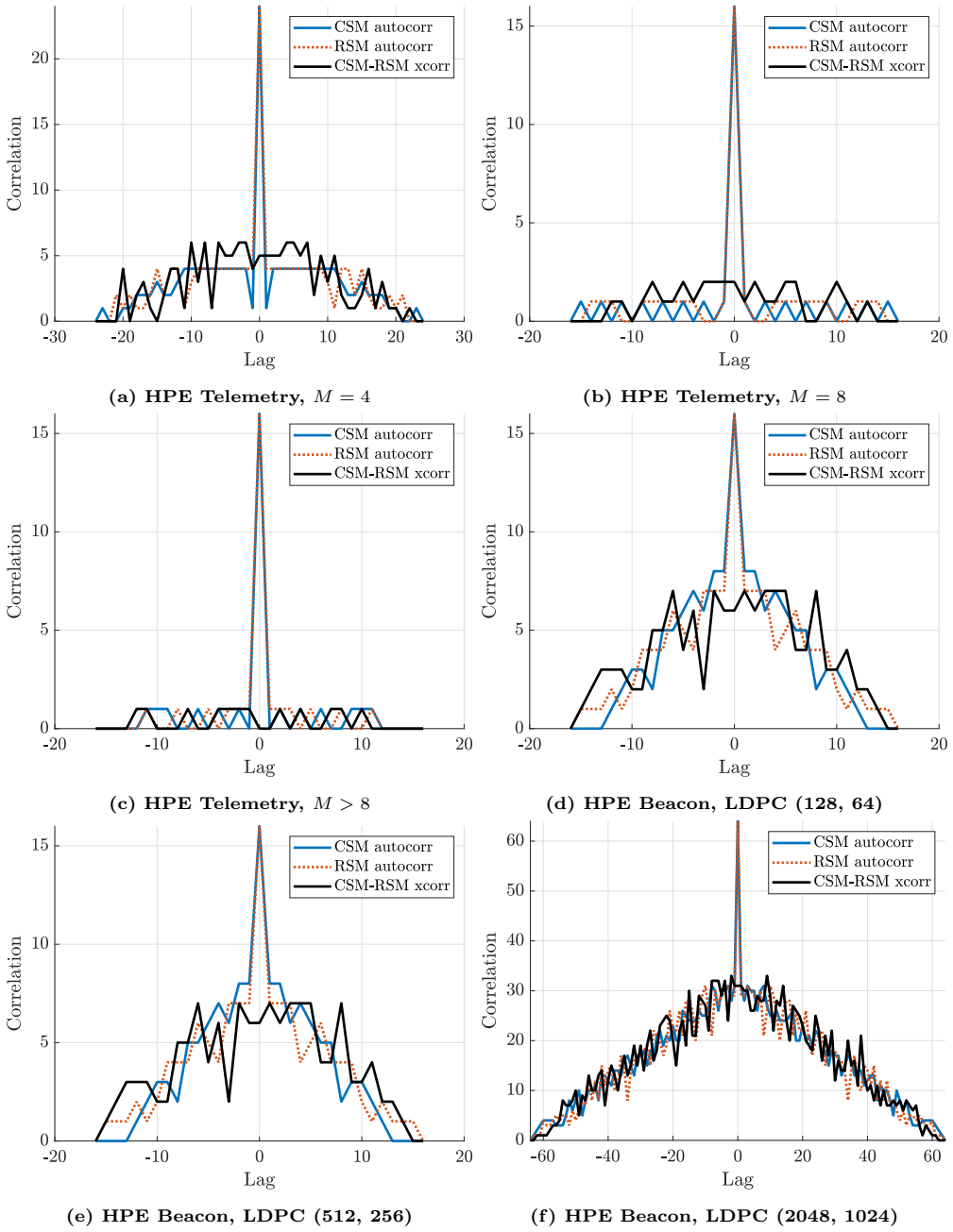

(a) HPE Telemetry, $M = 4$

(b) HPE Telemetry, $M = 8$

(c) HPE Telemetry, $M > 8$

(d) HPE Beacon, LDPC (128, 64)

(e) HPE Beacon, LDPC (512, 256)

(f) HPE Beacon, LDPC (2048, 1024)

Figure 8. Correlation Properties of the CSM and RSM. "LDPC" denotes Low-Density Parity-Check codes.

is synchronized with the ground-station clock. In other words, if the two clocks experience a drift, then Figure 9 should technically be updated to include additional blocks that model the dynamic nature of that drift. However, if we make the simplifying assumption that $t' = t + \Delta t$, where Δt is a constant (as will be done in the prototype described in Section IV), then the difference between t and t' does not meaningfully change the nature of our dynamic system and thus can be omitted from

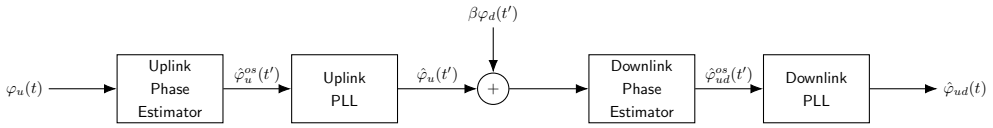

Figure 9. Synchronous Ranging System Model.

the analysis.

Because the uplink and downlink RCWs are synchronous, the phase at the ground station receiver is equal to the sum of the phase introduced by the downlink, expressed in uplink symbols and thus denoted by $\beta\varphi_d(t)$, and the uplink phase estimated by the spacecraft receiver:

$$\varphi_{ud}(t) = \varphi_u(t) + \beta\varphi_d(t). \tag{44}$$

Therefore, the phase estimator and PLL at the ground station track the uplink-plus-downlink dynamics to obtain the two-way phase estimate $\hat{\varphi}_{ud}(t)$.

To quantify the performance of the one-shot estimator on the uplink and downlink, we assume that it can be modeled as

$$\hat{\varphi}^{os}(t) = \varphi(t) + \varepsilon^{os}(t), \tag{45}$$

where $\varepsilon^{os}(t)$ denotes a possibly stochastic error of the phase estimate produced by the one-shot estimator. This error has a certain mean, or bias, as well as a given variance, which we will study in the next section. On the other hand, the uplink and downlink PLLs are assumed to be implemented digitally and thus are modeled using their discrete-time closed-loop transfer functions $H_u(z)$ and $H_d(z)$, which are expressed in the $\mathcal{Z}$-transform domain. Therefore, the overall system can be modeled as shown in Figure 10.

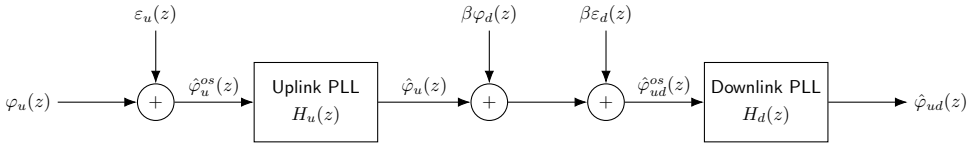

Figure 10. Synchronous Ranging System Model in the $\mathcal{Z}$-Transform Domain.

Also, by the principle of superposition, the overall system dynamics behavior are given by

$$\hat{\varphi}_u(z) = H_u(z)\left[\varphi_u(z) + \varepsilon_u(z)\right] \tag{46}$$

$$\hat{\varphi}_{ud}(z) = H_d(z)H_u(z)\left[\varphi_u(z) + \varepsilon_u(z)\right] + \beta H_d(z)\left[\varphi_d(z) + \varepsilon_d(z)\right]. \tag{47}$$

Therefore, the phase error on the uplink, and the uplink plus the downlink, becomes

$$e_u(z) = \varphi_u(z) - \hat{\varphi}_u(z) = \left[1 - H_u(z)\right]\varphi_u(z) - H_u(z)\varepsilon_u(z) \tag{48}$$

$$\begin{aligned} e_{ud}(z) = \varphi_{ud}(z) - \hat{\varphi}_{ud}(z) = &\left[1 - H_u(z)H_d(z)\right]\varphi_u(z) + \left[1 - H_d(z)\right]\beta\varphi_d(z) - \\ &H_d(z)\left[H_u(z)\varepsilon_u(z) + \beta\varepsilon_d(z)\right], \end{aligned} \tag{49}$$

and, consequently, the system behavior over time can be recovered by taking the inverse $\mathcal{Z}$-transform of the derived signals.

Note that, as currently stated, this model is only valid if the uplink and downlink PLLs have the same loop update rate (otherwise, their discrete transfer functions cannot be directly multiplied). To circumvent this problem, two scenarios are considered: First, if the ratio between the uplink and downlink PLL loop rate is rational, then the transfer function of the overall system can be obtained simply by upsampling the transfer function of the PLL running at the lowest rate. For instance, consider the case where the uplink PLL runs at a slower rate than the downlink PLL. Then the analysis previously developed remains valid, but $H_u(z)$ needs to be substituted by $H_u(z^{1/\beta})$ with β defined as before.

Alternatively, consider now a case where $\frac{1}{\beta}$ is not a rational number. Then the system performance can approximated by first upsampling $H_u(z)$ by a factor $K = \left\lfloor \frac{1}{\beta} \right\rfloor$ and then adjusting the rate of the resulting transfer function to the appropriate non-fractional value using a zero-order hold operation.

B. Bias of the Phase Estimate

This section focuses on understanding the sources of bias in the synchronous ranging system. In general, these biases are introduced by the combination of the one-shot phase estimator and the PLL so that

$$\bar{\varepsilon} = \bar{\varepsilon}_{os} + \bar{\varepsilon}_{pll}. \tag{50}$$

Note that for the downlink, this bias will be sum of bias in the uplink and the bias on the downlink, as expected.

Let us first consider the bias introduced in the uplink portion of the system and assume that the one-shot phase estimator integrates the received signal for T_{int} seconds prior to returning a phase estimate. Let t_1 and $t_2 = t_1 + T_{int}$ denote the start and end time of this integration period, respectively. Then, using the results from Appendix III, we know that

$$\tau_u(t_1) = \frac{1}{1-\gamma}\frac{d_0 + \gamma t_1}{c} \tag{51}$$

$$\tau_u(t_2) = \frac{1}{1-\gamma}\frac{d_0 + \gamma t_2}{c} = \frac{1}{1-\gamma}\frac{d_0 + \gamma(t_1 + T_{int})}{c}. \tag{52}$$

Therefore, the maximum phase error of the one-shot estimator is proportional to the difference in one-way light-time (OWLT) delay between the start and end of the integration period:

$$\Delta\varphi_u \propto \tau_u(t_2) - \tau_u(t_1) = \frac{\gamma}{1-\gamma} T^u_{int} \tag{53}$$

$$\Delta\varphi_d \propto \tau_d(t_2) - \tau_{ud}(t_1) \approx \frac{2\gamma}{1-2\gamma} T^d_{int}, \tag{54}$$

where T^u_{int} and T^d_{int} denote the uplink and downlink receiver integration times, respectively. Consequently, the steady-state bias introduced by the one-shot estimator is

$$\bar{\varepsilon}^{os}_u = \frac{\Delta\varphi_u}{T_u} = \frac{\gamma}{1-\gamma} N^u_{int} \tag{55}$$

$$\bar{\varepsilon}^{os}_{ud} = \frac{\Delta\varphi_u}{T_u} + \beta\frac{\Delta\varphi_d}{T_d} = \frac{\gamma}{1-\gamma} N^u_{int} + \beta\frac{2\gamma}{1-2\gamma} N^d_{int} \tag{56}$$

with N^u_{int} and N^d_{int} equal to the number of PPM symbols integrated on the spacecraft and ground station receiver, respectively. Observe that both $\bar{\varepsilon}^{os}_u$ and $\bar{\varepsilon}^{os}_{ud}$ are now expressed in units of uplink PPM symbols.

On the other hand, as shown in [8], the PLL may also introduce a bias in the form of a steady-state phase error. For a second-order PLL, this steady-state phase error is shown to be equal to [8]

$$\bar{\varepsilon}_{pll} \propto \frac{T^2_{int}}{K_i} \tau''_u(t), \tag{57}$$

where T_{int} denotes the PLL update rate, K_i is the PLL integration constant, and $\tau''_u(t)$ is the second derivative of the OWLT delay. Fortunately, if $d(t)$ is a linear function, then $\tau''_u(t) = 0$ and the PLL will not introduce any bias in the ranging system. Therefore, we conclude that

$$\bar{\varepsilon}_u = \bar{\varepsilon}^{os}_u \tag{58}$$

$$\bar{\varepsilon}_{ud} = \bar{\varepsilon}^{os}_{ud}. \tag{59}$$

Finally, corrections to this bias estimate are necessary if either the transmitter or the receiver apply range-rate compensation. For example, Appendix IV shows that if the receiver post-compensates the signal, then the formulas derived in this section are approximately correct, but the residual range rate $\epsilon_\gamma = \gamma - \hat{\gamma}$ must be used, where $\hat{\gamma}$ denotes the range rate predict obtainable from the spacecraft trajectory.

C. Variance of the Phase Estimate

Consider now the variance of the phase estimate resulting from combining a one-shot estimator and a PLL. To do so, we must invoke once again the principle of superposition of linear systems and constrain ourselves with just sources of stochastic randomness. These include jitter in the photon-arrival measurement introduced by the optical detector, as well as randomness caused by background noise.

Figure 11 shows a model of the sources of randomness in a two-way synchronous ranging system. In particular, we use the following notation:

- σ^2_{du} denotes the jitter introduced by the uplink photon detector, which we assume known a priori and expressed in units of uplink symbol time (i.e., if jitter

is expressed in seconds, divide the value by the uplink symbol duration and square it).

- σ_{nu}^2 denotes the variance of the one-shot phase estimator due only to the uplink channel signal and noise conditions.
- σ_u^2 denotes the variance of the phase estimate provided by the one-shot estimator on the uplink receiver.
- $k_u\sigma_u^2$ denotes the variance of the phase estimate provided by the PLL of the uplink receiver. The constant k_u is determined by $H_u(z)$, as shown later in this section.
- $\beta^2\sigma_{dd}^2$ denotes the jitter introduced by the downlink photon detector, which we assume known a priori and expressed in units of uplink symbol time. In other words, if the jitter is specified in seconds, divide the value by the downlink symbol time and multiply by β, then square the result.
- $\beta^2\sigma_{nd}^2$ denotes the variance of the one-shot phase estimator due only to the downlink channel signal and noise conditions, expressed in units of uplink symbol time.
- σ_d^2 denotes the variance of the phase estimate provided by the one-shot estimator on the downlink receiver.
- $k_d\sigma_d^2$ denotes the variance of the phase estimate provided by the PLL of the downlink receiver. The constant k_d is determined by $H_d(z)$, as shown later in this section.

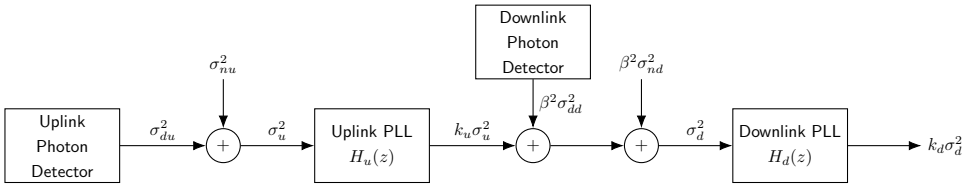

Figure 11. Variance Sources in a Synchronous Ranging System.

The variance of the one-shot estimator depends on the slot-synchronization algorithm used at the uplink and downlink receivers. For example, let us assume that both of them use a photon-counting detector with the Maximum-Likelihood (ML) estimator from [7] and [9]. Then it is shown in [9] that a lower bound on the variance of this estimator, measured in slots, is given by the Cramér-Rao Bound (CRB):

$$\sigma_{n*}^2 \geq \delta(1-\delta)\frac{K_s^2 + MK_sK_b + M^2K_b^2}{K_s^2\left(\frac{N_{int}}{M}K_s + 2N_{int}K_b\right)} = \frac{\delta(1-\delta)}{N_{int}T_s}\frac{\lambda_s^2 + \lambda_s\lambda_b + \lambda_b^2}{\lambda_s^2\left(\lambda_s + 2\lambda_b\right)}, \tag{60}$$

where

- $*$ in the subscript is used to indicate that the formula can apply to either the uplink or downlink if the corresponding values for the other parameters are used;

- δ is the fractional component of the timing offset at the receiver;
- λ_s and K_s denote the number of signal photons per second and per slot, respectively;
- λ_s and K_b denote the number of background noise photons per second and per slot, respectively;
- M is the PPM modulation order;
- and N_{int} is the number of symbols in one integration period.

Note that, as stated, this CRB depends on a parameter that cannot be known or predicted accurately in real operations, namely the fractional timing offset δ. There are two options to circumvent this problem: On the one hand, we can calculate the expectation over δ assuming its value has a uniform distribution between 0 and 1. On the other hand, we can calculate the worst-case CRB by calculating the value of δ that maximizes it. This latter approach leads to

$$\sigma_{n*}^2 \geq \frac{1}{4}\frac{1}{(M+P)^2}\frac{1}{N_{int}T_s}\frac{\lambda_s^2+\lambda_s\lambda_b+\lambda_b^2}{\lambda_s^2\,(\lambda_s+2\lambda_b)}, \tag{61}$$

whereas the expectation approach leads to the same result but with a factor 1/6 instead of 1/4. Furthermore, in this latter expression we have applied a correction factor of $1/(M+P)^2$ so that the resulting variance is expressed in units of PPM symbols instead of slots.

Next, we focus our attention on estimating the expected variance at the output of the PLL. More specifically, this section explains how to calculate the constants k_u and k_d that relate the input and output variance depending on the PLL closed-loop transfer functions. Note that if either $H_u(z)$ or $H_d(z)$ have been upsampled or resampled to rate-match the uplink and downlink PLLs as explained in Section III.A, then the PLL transfer functions resulting from that operation must be used instead. However, the notation does not reflect this change for simplicity's sake.

It is well known that the PLL can be viewed as a low-pass filter. Therefore, the variance of the phase estimator is directly related to the uplink loop noise bandwidth, which, in the case of the uplink, is defined as

$$2B = \int_{-1/2T_{int}}^{1/2T_{int}} |H_u(e^{j2\pi f T_{int}})|^2 df, \tag{62}$$

where B denotes the one-sided PLL loop bandwidth. Using the transformation $z = e^{j2\pi f T_{int}}$, this equation can be rewritten as

$$2BT_{int} = \frac{1}{2\pi j}\oint_C H_u(z)H_u(z^{-1})z^{-1}dz, \tag{63}$$

where C is a closed path along the unit circle and, thus, $z^* = z^{-1}$. We can now use the residue theorem to obtain

$$2BT_{int} = \sum_{\forall z_i} \text{Res}\left(H_u(z)H_u(z^{-1})z^{-1}, z_i\right), \tag{64}$$

where the summation is performed over all poles z_i of $H_u(z)$, and $\text{Res}\left(f(z), c\right)$ denotes the residue of the function $f(z)$ with respect to the pole c:[12]

$$\text{Res}\left(f(z), c\right) = \begin{cases} \lim\limits_{z\to c}(z-c)f(z) & \text{if } c \text{ is a simple pole} \\ \frac{1}{(n-1)!}\lim\limits_{z\to c}\frac{d^{n-1}}{dz^{n-1}}(z-c)^n f(z) & \text{if } c \text{ is a pole of order } n. \end{cases} \tag{65}$$

For example, if $H_u(z)$ is a second-order PLL, it is shown in [8] that its closed-loop transfer function is equal to

$$H(z) = \frac{(K_p + K_i)z - K_p}{z^2 + (K_p + K_i - 2)z - 1 + K_p}, \tag{66}$$

where K_p and K_i denote the proportionality and integrate constants of the PLL. Therefore, following the procedure outlined above, results in [8]

$$k_* = 2BT_{int} = \frac{2K_p^2 + 2K_i + K_pK_i}{K_p(4 - 2K_p - K_i)}, \tag{67}$$

where $*$ indicates that the formula is valid for both the uplink and the downlink provided the corresponding values for each link are used. Finally, once k_u and k_d have been determined, the variance of the phase estimate at the output of the synchronous ranging system will be

$$\sigma_{ud}^2 = \underbrace{k_d k_u \left(\sigma_{du}^2 + \sigma_{nu}^2\right)}_{\text{Uplink contribution}} + \underbrace{\beta^2 k_d \left(\sigma_{dd}^2 + \sigma_{nd}^2\right)}_{\text{Downlink contribution}}. \tag{68}$$

Note that σ_{ud}^2 is now expressed in units of uplink symbols. Note also that for a well-designed system, both the PLL of the uplink and downlink receivers are typically sized so that $B_uT_{int} \leq 0.1$. Consequently, k_u and k_d are approximately ≤ 0.2 and, therefore, $k_dk_u \ll k_d$. Therefore, if both the uplink and downlink operate at approximately the same symbol rate, then the ranging performance is dominated by the noise conditions on the downlink. If, on the other hand, the downlink runs several orders of magnitude faster than the uplink, then $k_u \gg \beta^2$ and noise on the uplink becomes the limiting factor.

D. Accuracy and Precision of the Range Estimate

The output of the PLL synchronizer can be used to estimate both the PPM symbol clock and the phase of the received signal. In particular, once per update time of the

[12] The poles of $H_u(z^{-1})$ do not contribute to the contour integral because they lie outside of the unit circle. Similarly, there is no pole at $z = 0$ due to the z^{-1} term [8].

PLL, the slot synchronizer generates an estimate of the relative phase $\hat{\varphi}_R$. We denote the set of discrete samples generated by the PLL as $\{\hat{\varphi}_R\}$.

Any given sample in $\{\hat{\varphi}_R\}$ is computed by integrating the received signal during $N_{int}T$ seconds, where N_{int} has been configured so that the change in OWLT during this integration period is negligible (e.g., 1/10 of a slot). Therefore, the PPM symbol associated with the k-th sample of $\{\hat{\varphi}_R\}$ is approximately equal to the mid-point of the integration period. Thus, at the output of the slot synchronizer we can construct a time series $\left\{\hat{t}_R, \hat{\psi}_R\right\}$ where the k-th entry is equal to[13]

$$\hat{t}_R[k] = T\left(k + \hat{\varphi}_R[k]\right) \tag{69}$$

$$\hat{\psi}_R[k] = (k+1)\tfrac{N_{int}}{2}. \tag{70}$$

These measurements can now be used directly in Equation (30) to recover the range between the spacecraft and the ground station, or interpolated as necessary if range estimates are required at higher sampling rates.

The equations presented in this section also clarify how the error analysis from Sections III.B and III.C affects the range measurement. In particular, the timing error due to imperfect PLL tracking will be

$$\varepsilon_{t_R} = \hat{t}_R - t_R = T_u \varepsilon_{ud}, \tag{71}$$

where $\varepsilon_{ud} = \hat{\varphi}_{ud} - \varphi_{ud}$, and we use the uplink PPM symbol plus guard time T_u as a multiplicative factor, because throughout this section, we have consistently used uplink PPM symbols as our unit of choice. Therefore, the bias and standard deviation in the RTLT measurement is simply[14]

$$\bar{\varepsilon}_{\tilde{\tau}_{ud}} = T_u \bar{\varepsilon}_{ud} \tag{72}$$

$$\sigma_{\tilde{\tau}_{ud}} = T_u \sigma_{ud}. \tag{73}$$

Finally, to calculate the uncertainty of the range estimate, additional factors must be considered (e.g., speed of light being nonconstant in Earth's atmosphere). For example, in the simple case of linear motion as assuming no delays onboard the spacecraft, we can use Equation (38) to get

$$\bar{\varepsilon}_{range} = \tfrac{c}{2} T_u (1+\gamma) \bar{\varepsilon}_{\tilde{\tau}_{ud}} \tag{74}$$

$$\sigma_{range} = \tfrac{c}{2} T_u (1+\gamma) \sigma_{\tilde{\tau}_{ud}}, \tag{75}$$

where the value of γ can be approximated by its predict $\hat{\gamma}$ or estimated in conjunction from the range from the available data. Note that if rate post-compensation is applied, then this formula is modified to only account for the residual range rate experienced by the PLL synchronizer, as shown in Appendix IV.

---

[13] This time series is assumed to use zero-based indexing.

[14] Note that the ranging system measures $\tilde{\tau}_{ud}(t_R)$ rather than $\tau_{ud}(t_T)$, but the latter can be recovered in post-processing.

IV. Prototype Description

This section describes a software-based prototype of the synchronous ranging system described in Section II. In particular, the discussion is divided in two parts. First, this section discusses the overall prototype architecture, including special precautions that must be taken into account when working in simulated time. Second, it details the different functionality that needs to be implemented in the prototype in order to fully exercise the synchronous ranging system.

A. Prototype Architecture

Figure 12 provides a high-level block diagram of all the functionality that needs to be implemented to prototype a synchronous ranging system. This includes the ground station uplink and downlink subsystems, as well as the spacecraft transmit and receive subsystems, and the uplink and downlink optical channels. Details on each of them are provided later in this section.

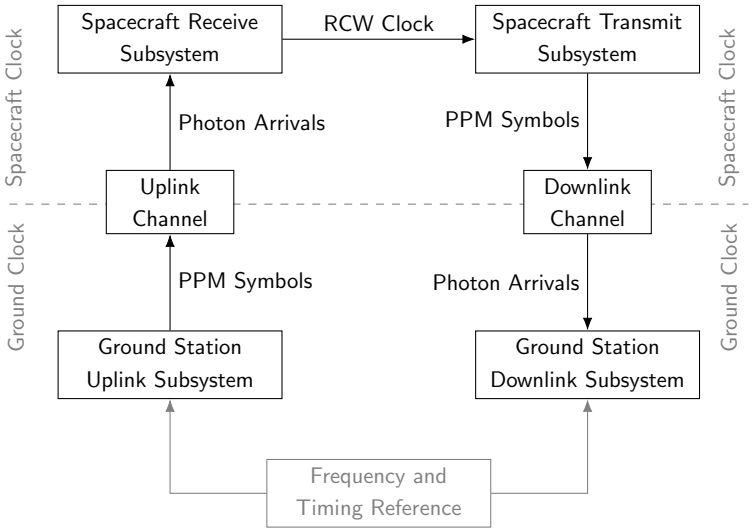

Figure 12. High-Level Functionality for a Synchronous Ranging System.

Figure 12 shows that a common frequency and timing reference must be available at the ground station to recover range measurements. While this is necessary in a real-life, hardware-based implementation of the system, a software simulation does not need to include it because a common simulation time reference across multiple simulation components can be easily shared.

Finally, because the goal of a ranging system is not to transmit data but rather to obtain observables that can then be converted into estimates of the RTLT delay, the prototype does not require actual bits to be encoded and decoded. Instead, the focus of implemented functionality is related to slot, symbol, and RSM synchronization.

B. Prototype Functionality

1. Spacecraft vs. Ground-Station Clock

Care must be exercised when prototyping a synchronous ranging system in simulation to ensure that "additional" (and unavailable) information is not provided to the spacecraft receiver. In particular, in a real system implementation, the spacecraft clock is asynchronous from the ground-station clock and regulated independently by the spacecraft ultra-stable oscillator (USO), which drifts randomly. Therefore, when working in a simulated environment, additional processing effort must be spent to ensure that a common time reference is not shared between the ground station and the spacecraft.

To achieve that goal, the prototype defines separate measures of time for the spacecraft and ground station (see Figure 12). In other words, it is as if the system has two units of time, "spacecraft seconds" (denoted here by t_{sc}) and "ground-station seconds" (denoted by t_{gs}), and the relationship between the two variables establishes the level of synchronicity between the spacecraft and the ground-station clock.

For example, if $t_{sc} = t_{gs}$, then the spacecraft and ground-station clocks are synchronized—a condition that is not realistic but is useful for debugging purposes. Alternatively, one might select a simple time-shift to model a lack of synchronicity, i.e.,

$$t_{sc} = t_{gs} + \Delta t, \tag{76}$$

where Δt is an arbitrary constant that is selected randomly prior to the start of the simulation. Clocks are also known to have long-term frequency drifts. While this could also be modeled in the prototype, it was left out of scope for the sake of simplicity.

In the prototype, the transformation between t_{sc} and t_{gs} is applied by the uplink and downlink optical channels. In particular, the uplink optical channel takes as input the set of times at which a PPM symbol starts departing from the ground station, in ground-station seconds, and transforms that value to the time of arrival of different photons for that slot, corrected by the uplink OWLT delay and expressed in spacecraft seconds. Similarly, the downlink optical channel takes as input the departure times of downlink PPM symbols in spacecraft seconds and outputs photon-arrival times at the ground station, corrected by the downlink OWLT delay and expressed in ground-station seconds.

2. Ground Station Uplink Subsystem

The ground-station uplink subsystem takes as input a set of configuration parameters and generates a sequence of PPM symbols that are compatible with either the CCSDS HPE telemetry standard or the CCSDS HPE beacon-plus-accompanying-data standard. The exact set of processing steps performed to generate this sequence of PPM symbols is provided in [5].

The prototype also includes an extra configuration parameter to indicate the number N_u of SMCWs per RCW. Similarly, it also includes the necessary functionality to replace the CSM in 1 out of N_u SMCWs with the corresponding RSM, as provided in Appendix I.

Finally, the ground-station uplink subsystem also determines the instants of time at which each PPM symbol departs from the ground station. For the sake of simplicity, I assume these to not be range-rate pre-compensated, so consecutive PPM symbols depart after $T = (M + P)T_s$ seconds have elapsed.

3. Uplink Channel

The uplink channel takes as input the set of PPM symbols transmitted by the ground station, as well as the time they start departing, and calculates photon-arrival times that are Poisson-distributed and corrected by the OWLT. In particular, the uplink channel performs the following steps:

1. Calculate the number of noise photons that arrive in each empty slot by sampling a Possion distribution with mean K_b.

2. Calculate the number of signal photons that arrive in each signal slot by sampling a Possion distribution with mean $K_s + K_b$.

3. Calculate the time of departure of all photons within a given slot by sampling a uniform distribution between 0 and T_s as many times as indicated by the result of steps (1) and (2).

4. For each photon departure, calculate the photon arrival as $t_{arr} = t_{dep} + \tau(t_{dep})$. For simplicity's sake, the prototype assumes that both $\tau_u(t) = \tau_0 + \gamma t$ and $\tau_d(t) = \tau_0 + \gamma t$ so that $\tau_{ud}(t) = \tau_u(t) + \tau_d(t + \tau_d(t)) = (2 + \gamma)(\tau_0 + \gamma t)$. This is not exactly the same result obtained under linear motion in Appendix III, but it is a good approximation when $\gamma \ll 1$ and allows us to implement a single channel function and reuse it for both the uplink and the downlink.

5. Transform the time of arrival of each photon from ground-station seconds to spacecraft seconds by applying a Δt correction.

6. Transform the time of arrival of each photon from spacecraft seconds to a sample index by multiplying it by 64 GHz. This last step is optional and allows us to store photon arrivals as unsigned integers for increased precision, rather than rely on floating point numbers. Furthermore, this conversion provides a time resolution of 15.62 ps, which is sufficient to achieve a ranging accuracy of 4 mm, which is negligible for the purposes of the prototype.

4. Spacecraft Receiver Subsystem

The spacecraft receiver implemented in the prototype is based on the architecture developed at JPL for the Deep Space Optical Communications (DSOC) experiment. It is based on a photon-counting detector that is connected to a time-tagging device. This time tagger outputs a timestamp every time a photon arrives. The collected timestamps are then processed to achieve slot, symbol, and RSM synchronization.

Figure 13 depicts the different parts of the receiver implemented in the prototype. Blocks color-coded in gray are not explicitly included in the simulation because time tags for the photon arrivals are generated by the optical uplink and downlink channels.

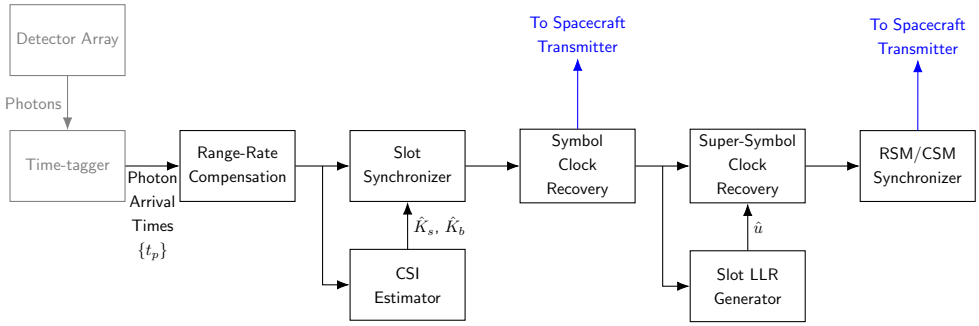

Figure 13. HPE Receiver Architecture. "CSI" and "LLR" stand for Channel State Information and Log-Likelihood Ratio, respectively.

Note that in Figure 13, the spacecraft receiver provides the spacecraft transmitter with both the symbol clock and the RSM clock. This contradicts Figure 12, in which only the RSM clock is shared between the transmitter and receiver. Technically, while only the latter is needed, the prototype actually shares both clocks to improve the level of synchronization between the spacecraft uplink and downlink clocks. However, neither of those clocks is shared with the parts of the prototype that implement the ground station, thus ensuring that there is no synchronicity between the spacecraft and ground station.

Finally, a detailed explanation of the different algorithms used in the receiver is beyond the scope of this paper. Instead, see references [7] and [10] for details on the signal-processing steps performed in each block of Figure 13. Similarly, details on range-rate compensation are provided in Appendix IV.

5. Spacecraft Transmitter Subsystem

The spacecraft transmitter is implemented using the same functionality as the ground-station uplink subsystem. However, the time of departure of each downlink PPM symbol is regimented by the clock recovered from the spacecraft receiver, which is shown in Figure 13 in blue. Therefore, the slot departure times are no longer equal

to $T = (M + P)T_s$ seconds but rather are time-varying and determined by $\tau_{ud}(t)$.

6. Downlink Channel

The downlink channel uses the same procedures as the uplink channel, except it converts from spacecraft seconds to ground-station seconds by applying the inverse time offset Δt. It uses the same linear approximation to calculate the time of arrival of each photon at the receiver so that the total RTLT delay becomes

$$\tau_{ud}(t_T) = (2 + \gamma)(\tau_0 + \gamma t_T), \tag{77}$$

which is approximately equal to the exact $\tau_{ud}(t_T)$ expression provided in Appendix III.

7. Ground-Station Downlink Subsystem

The ground-station downlink subsystem is implemented using the same functional blocks as the spacecraft uplink receiver. However, the configuration parameters affected by the spacecraft range rate are modified to account for the fact that, on the downlink, the apparent range rate experienced by the receiver is twice the actual range rate.

C. Prototype Implementation

The prototype described in this section has been implemented in MATLAB using a combination of functions and classes, some of which have been compiled to C for faster execution. All inputs are provided via a single configuration file, which returns a structure that contains general parameters (e.g., location where results should be stored) as well as parameters specific to the uplink and downlink transmitter, channel, and receiver. This structure is then populated with additional values and checked for consistency prior to starting the simulation.

The prototype can operate in two modes, one mostly intended for debugging purposes and another that has been optimized to perform long simulation runs. In debug mode, the spacecraft and ground-station clocks are synchronized to facilitate debugging. Furthermore, the entire simulation is run sequentially and all information is stored in memory. Consequently, the amount of random-access memory (RAM) in the host computer becomes the limiting factor that dictates whether a simulation can be performed or not. Note that this is particularly limiting when simulating links with high modulation orders (as is the case for deep space operations) and high signal and noise conditions. Indeed, in these circumstances the number of photons simulated becomes increasingly large, thus making it more likely that the host will run out of RAM.

The secondary mode of operations is based on MATLAB classes. This allows the prototype to run in an iterative fashion, using the internal class variables to store the

necessary state information across iterations. Furthermore, in this mode of operations the prototype lifts the restriction that the spacecraft and ground-station clocks be synchronized, thus allowing us to better simulate the actual conditions under which the ranging system would operate.

Finally, the output of the simulation includes the following files:

- Uplink-transmitted symbols: This file contains a list of all PPM symbols and their departure times in ground-station seconds. The file also includes a marker to indicate the start of each RCW.
- Uplink-received photons: This file contains a list of all photon arrivals to the spacecraft, corrected for the OWLT and expressed in spacecraft seconds.
- Downlink-transmitted symbols: This file contains a list of all PPM symbols to be sent in the downlink. The departure times may optionally be recorded as well in spacecraft seconds.
- Downlink-received photons: This file contains a list of all photon arrivals at the ground station in ground-station seconds.

Additionally, all information produced by the ground station is stored, including the recovered symbol and super-symbol clock, as well as the measured time of arrival of each RSM.

V. Results

A. Scenario Description: The DSOC Terminal

To test the synchronous ranging simulator, I collected information on the planned trajectory for the DSOC terminal and the Psyche spacecraft. In particular, I obtained copies of the spacecraft trajectory and its communications subsystem and calculated, from them, realistic uplink and downlink channel conditions.

Figure 14 shows the range and range rate profile for the Psyche spacecraft over time. Observe that during certain phases of the spacecraft's range rate normalized by the speed of light, γ, can be as high as $7.7 \cdot 10^{-5}$, approximately, so the duration of a slot as received by the ground station increases by 0.0154%. However, in the simulations I assume that the receiver post-compensates the range rate with sufficient accuracy so that the residual range rate is just 100 m/s, approximately, a value that is realistic for mission phases in which no impulsive maneuvers or planetary entries are being performed.

To quantify the uplink channel conditions, I assumed that the uplink is established between the JPL Optical Communications Telescope Laboratory (OCTL) and the DSOC terminal. The former has a 1-m telescope connected to a system of lasers

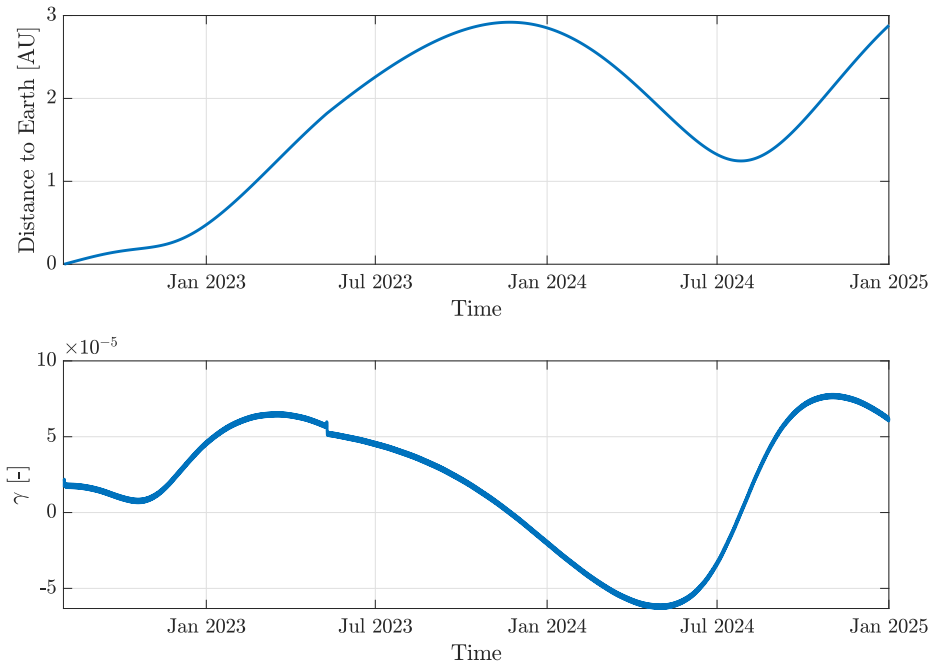

Figure 14. Range and Range Rate for the Psyche Spacecraft.

capable of providing 5 kW of optical power, while the latter carries a 22-cm aperture. For the downlink, I assumed transmission to the Palomar Observatory telescope, which is equipped with a 5-m aperture. All these inputs were provided to the JPL Strategic Optical Link Tool (SOLT) [11], which then estimated the optimal modulation parameters to maximize the link data rate (and thus not necessarily match the actual settings of DSOC when in flight).

Figures 15a and 15b show the estimated performance of the uplink and downlink, respectively. For the uplink, I report the Sun-probe-Earth (SPE) angle, while on the downlink I provide estimates of the Sun-Earth-probe (SEP) angle. In both cases, I also provide estimates of the signal and noise photon flux rate λ_s and λ_b for the first two years of the mission, as well as estimates of the achievable data rate.

This information can now be used to obtain a range-error estimate if I assume that both the spacecraft and the ground station utilize a photon-counting receiver like the one described in Section IV.[15] Figure 16 shows the results of this analysis assuming that the detectors onboard the spacecraft and the ground station have a jitter equal to 10% of the minimum supportable slot duration [4]. Results indicate that the ranging accuracy is mostly driven, as expected, by the distance between the transmitter and receiver, as well as the SEP angle.

[15] The author is aware that a real spacecraft receiver would not necessarily utilize a photon-counting device as a ground station would, but I used this assumption to simplify the prototype implementation.

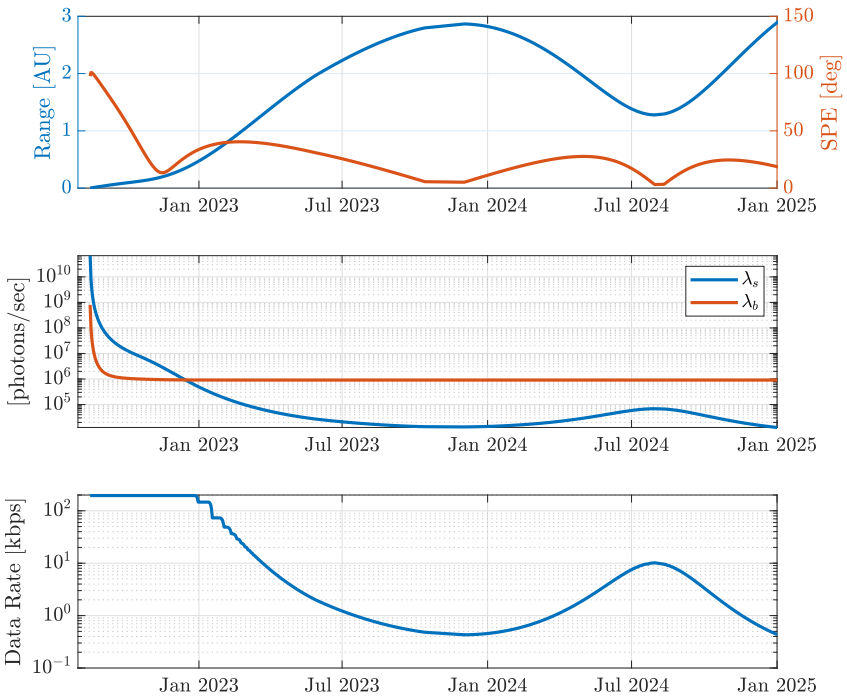

(a) Uplink Channel between OCTL and DSOC

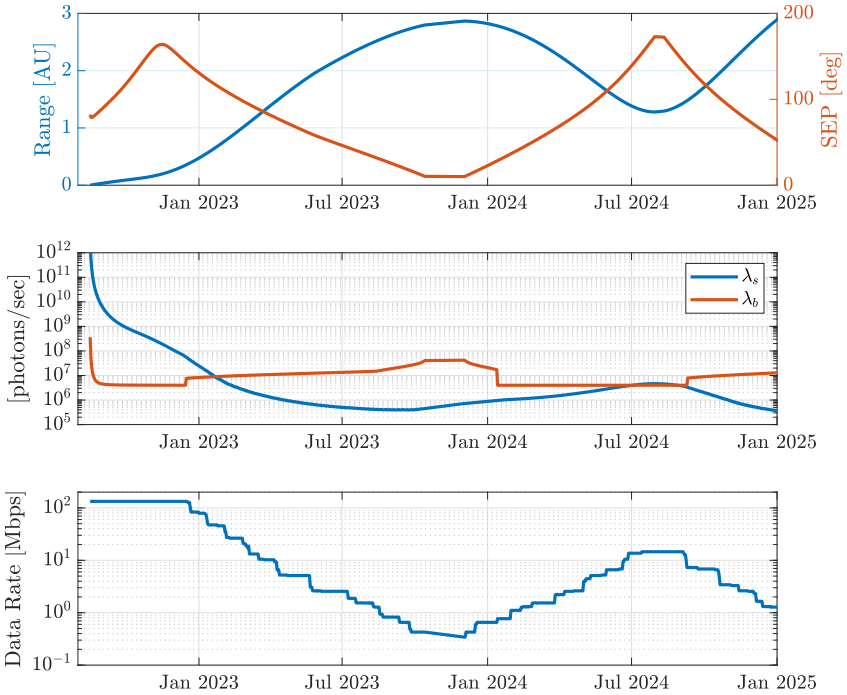

(b) Downlink Channel between DSOC and Palomar

Figure 15. Uplink and Downlink Channels for DSOC.

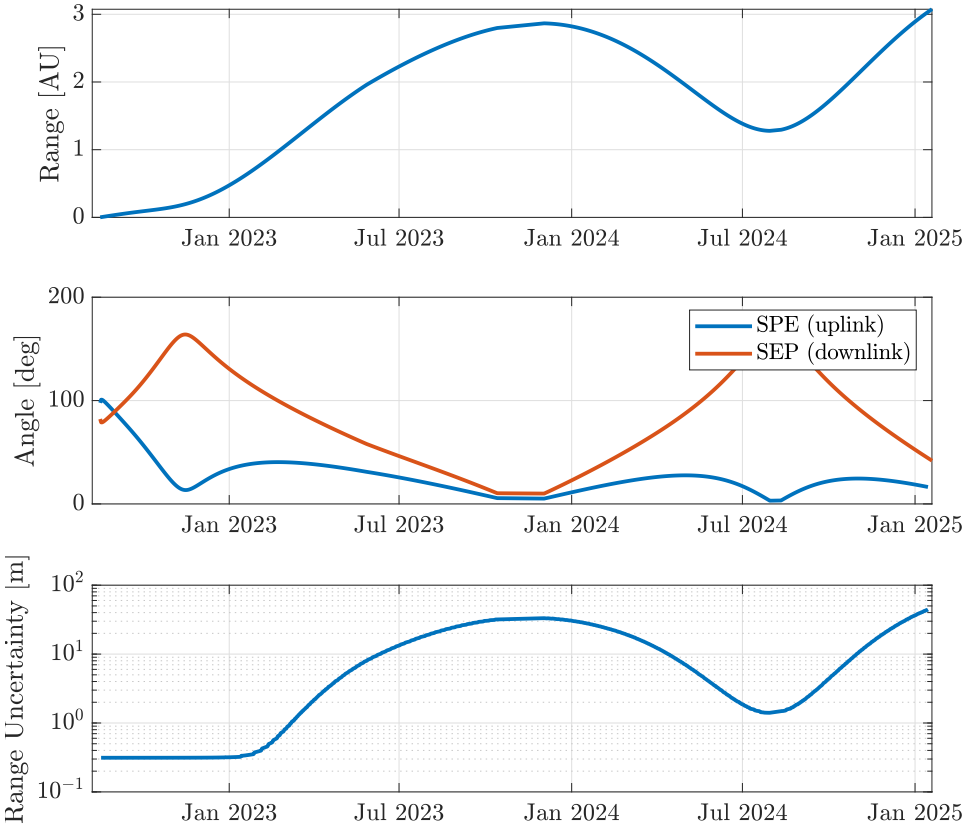

Figure 16. Expected DSOC Range Uncertainty.

Using this information, I construct two test cases to test and validate the synchronous ranging prototype. The first test illustrates the performance of the system during its transient state and is compared against the theoretical performance derived in Section III. It exercises the synchronous ranging system at high-signal and low-noise conditions, thus providing a best-case estimate of the overall system performance. However, it is not necessarily representative of DSOC operations.

The second case study, on the other hand, is selected to illustrate ranging performance with DSOC when operating at 1 AU. It exercises the ranging system assuming that both the uplink and downlink use HPE telemetry. Furthermore, I assume that both the spacecraft and the ground station perform range-rate post-compensation, resulting in a residual range rate of 150 m/s approximately, which is reasonable given the expected accuracy of the DSOC trajectory predicts.

B. Test Case 1: Validation

1. Inputs

In this validation exercise, I considered a system in which both uplink and downlink transmit use HPE telemetry. The uplink data rate is 1 Mbps approximately, while the downlink data rate is 33 Mbps. Note that this configuration does not necessarily match the expected DSOC operations. Instead, in this test I seek to exercise all the functionality of the prototype under benign channel conditions, which allows me to easily detect errors in the prototype and provides an estimate for the best-case range error performance.

The exact configuration parameters used during the simulation are provided in Table 1. Note that in this scenario, K_s, K_b, and the range rate were obtained from Figures 14, 15a, and 15b based on the predicted trajectory and signal-flux conditions on October 9, 2022, which results in fairly high signal-to-noise conditions. Thus, I only require the receiver to integrate 512 PPM symbols prior to obtaining a phase estimate.

Table 1. Configuration Parameters for Test Case 1.

Parameter	Uplink	Downlink	Units
Signal photons per slot (K_s)	10.24	21.44	photons/slot
Noise photons per slot (K_b)	0.064	0.008	photons/slot
Residual range rate ($r - \hat{r}$)	125	125	m/s
Slot width (T_s)	64	2	ns
Modulation order (M)	16	16	-
Repeat factor (Q)	1	2	PPM symbols
Code rate	1/3	2/3	-
Information rate	1.03	33.08	Mbps
No. of CW per RCW (N)	1	16	-
No. symbols integrated (N_{int})	512	512	PPM symbols

Note that I somewhat arbitrarily set the repeat factor of the downlink to $Q_d = 2$. This is not really necessary because, as previously stated, the signal conditions are favorable, and thus there is no need to artificially reduce the data rate by a factor of 2 in order to increase the number of photons per received symbol. However, this setting allows one to test the simulator functionality that recovers the timing of each super-symbol, a step that would not be required if both uplink and downlink had the repeat factor set to 1.

With the configuration of Table 1, each uplink codeword lasts for 4.85 ms, approximately. Furthermore, because each RCW only contains one uplink codeword, this time is also equal to the duration of a RCW. On the other hand, each downlink

codeword only lasts 0.30 ms, so 16 codewords are necessary to create a ranging codeword that lasts for 4.85 ms.

Finally, combining the channel conditions on October 9, 2022 together with the uplink configuration parameters of Table 1 and the equations presented in Section III allows us to calculate the expected range precision for the scenario. In particular, the theoretical results indicate that a range error of 1.7 cm should be expected.

2. Results

The results of this analysis are provided in Figure 17, which shows the error at the receiver for both the uplink and downlink channel. Three figures of merit are provided: error in slot phase estimation, error in detection of the start of a super-symbol, and error in detection time of an RSM. For the first metric, three plots are provided: the slot-synchronization error as measured during the simulation; the expected error from the theoretical analysis in Section III; and the expected steady-state error due to the ML estimator, also provided in Section III.

Observe that the agreement between the simulation results and the analytical results is excellent, both in terms of the steady-state error and the transient behavior of the one-way and two-way synchronous ranging systems. In both cases, the receiver clearly synchronizes its slot clock to the incoming signal and tracks the residual range rate at the expected steady-state error. Furthermore, the steady-state RSM timing error (expressed in meters) at the ground station receiver (i.e., both uplink and downlink) is as low as 1 mm, indicating that the performance of the system is excellent (for reference, a ranging error of 1 m is typical for deep space navigation with the DSN). In fact, in this scenario the measured ranging error is so small that it is likely that calibration errors not modeled in the simulation would become dominant in actual operations.

C. Test Case 2: HPE Telemetry on Uplink and Downlink

1. Inputs

This test case exercises a synchronous ranging system under representative deep space conditions. In particular, I assume that a ranging measurement is to be obtained with DSOC when operating at 1 AU on February 25, 2023. The exact simulation parameters are provided in Table 2. Compared to the previous test case, the PPM modulation order has been increased to $M = 128$, the maximum setting supported by DSOC, and the integration time has been increased to 2048 PPM symbols. Note that this increase is possible because, as previously mentioned, the trajectory predicts provide a range-rate estimate that is accurate to 150 m/s approximately, and both the spacecraft receiver and the ground station receiver implement range-rate post-compensation.

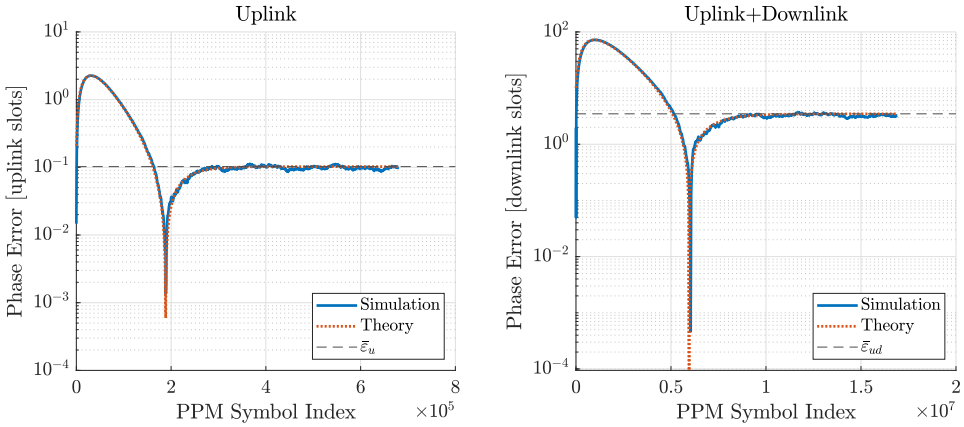

(a) Phase Error in the Slot Synchronizer

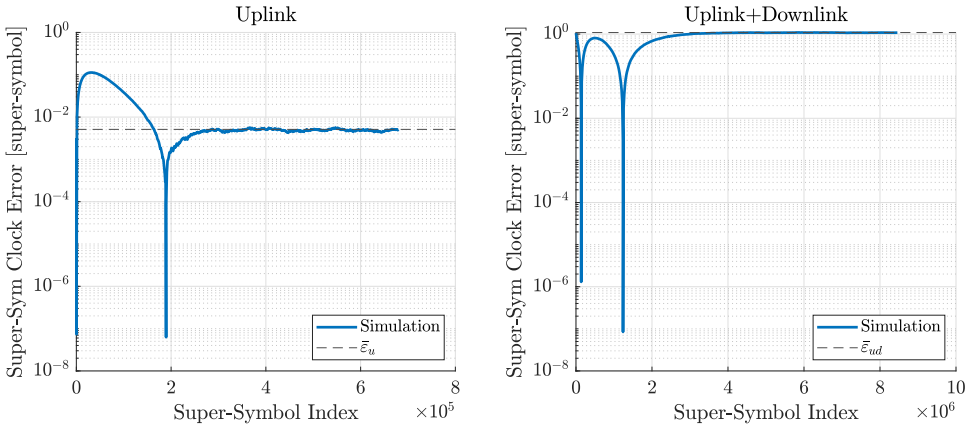

(b) Super-Symbol Timing Error

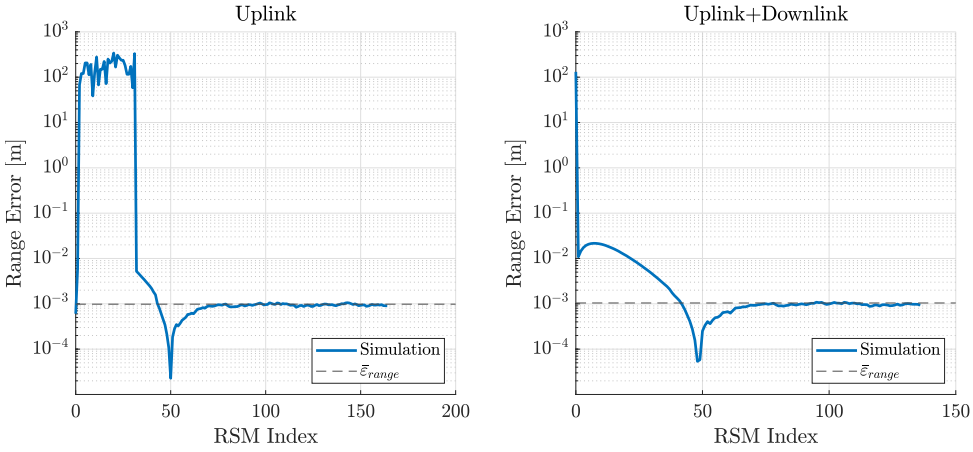

(c) RSM Timing Error

Figure 17. Results for Test Case 1.

The result of this configuration is an uplink that operates at 15 kbps approximately, while the downlink operates at 3.6 Mbps. Thus, synchronicity between the uplink and

Table 2. Configuration Parameters for Test Case 2.

Parameter	Uplink	Downlink	Units
Signal photons per slot (K_s)	6.86	1.34	photons/slot
Noise photons per slot (K_b)	0.47	0.04	photons/slot
Residual range rate ($r - \hat{r}$)	125	125	m/s
Slot width (T_s)	512	4	ns
Modulation order (M)	128	128	-
Repeat factor (Q)	2	1	PPM symbols
Code rate	1/3	1/3	-
Information rate	0.014	3.6	Mbps
No. of CW per RCW (N)	1	256	-
No. symbols integrated (N_{int})	2048	2048	PPM symbols

downlink clocks must be maintained despite the fact that there are three orders of magnitude difference between the uplink and downlink data rate. Also, the duration of one uplink CSM-marked codeword is 356.5 ms approximately, while a downlink codeword only lasts for 1.392 ms. Therefore, each downlink RCW will contain 256 codewords.

The expected performance of the system can be computed using the equations provided in Section III, which results in a range uncertainty estimate of 2.23 m, a value that is significantly larger than in the previous test case due to reduced signal conditions on the downlink.

Finally, I assume that at the start of the ranging pass, the spacecraft is at 1 AU from the ground station. Therefore, the initial OWLT is 498.66 seconds approximately. In a full ranging system, the time of detection of the RSMs is used to disambiguate the range to the spacecraft. However, for the purposes of this prototype, I assume that this step is not necessary and instead focus only on the ability of the system to track the spacecraft dynamics modulo the uplink symbol time. In other words, I set the initial OWLT to 498.66 s modulo the uplink symbol time, i.e., $2.56 \cdot 10^{-7}$.

2. Results

The range error resulting from the synchronous ranging system is plotted in Figure 18 for a total simulation of two minutes approximately. Additionally, the theoretical estimates for the 1-sigma and 3-sigma range precision are provided for reference. Note that to construct Figure 18, the bias in the range estimate introduced by the synchronous ranging system has already been removed, so the provided values represent the residual error due to stochastic sources.

Results indicate that it takes approximately a minute to a minute and a half for the

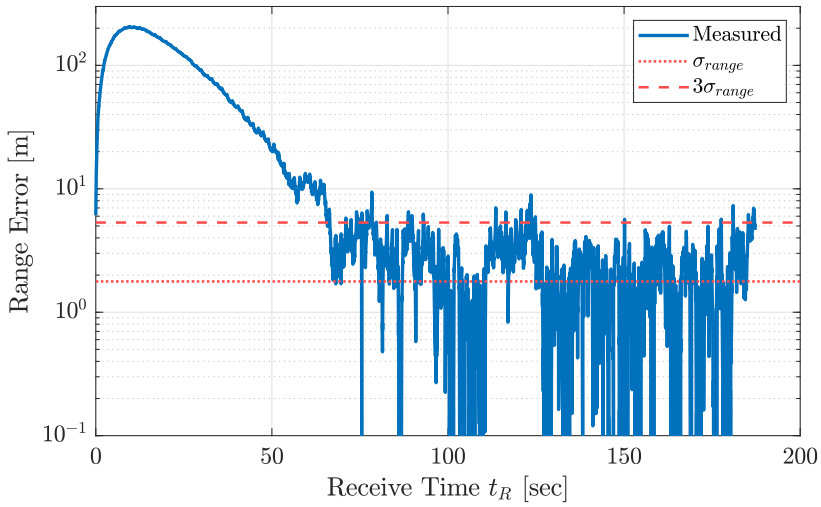

Figure 18. Expected DSOC Range Uncertainty.

PLL in the ground station to fully lock onto the downlink signal. Once lock is achieved, the ranging system provides estimates of the spacecraft range that agree well with the expected system performance.

VI. Conclusions and Future Work

This article describes a synchronous optical ranging system that can be used to determine the range between a spacecraft and a ground station when both the uplink and downlink communications are established using an optical link. In particular, it provides a description of the concept of operations and which parts of the CCSDS protocol stack need to be modified to be able to support simultaneous ranging and data transmission. This article also derives theoretical equations to determine the expected system performance (range precision and accuracy) as a function of the optical link budget parameters. It also describes a software-based prototype that demonstrates its operation.

This article presents results for two scenarios that are representative of significantly different operational conditions. The first scenario is used as an initial validation exercise for the software prototype and thus assumes favorable signal and noise conditions. As a result, the ranging system is able to recover range estimates with residual errors well below 1 m. The second scenario, on the other hand, shows the performance in a more challenging scenario in which the spacecraft is at 1 AU from the ground station. In this case, ranging errors on the order of $\sim$1 m are expected based on the derived theoretical results, a value that agrees well with the simulations.

Acknowledgments

I would like to acknowledge Jon Hamkins and Ryan Rogalin for their thorough review and significant contributions to this article. I would also like to acknowledge Abhijit Biswas and Meera Srinivasan for providing trajectory information for DSOC.

The research was carried out at the Jet Propulsion Laboratory, California Institute of Technology, under a contract with the National Aeronautics and Space Administration (80NM0018D0004).

References

[1] M. Sanchez Net and J. Hamkins, "Optical Telemetry Ranging," *The Interplanetary Network Progress Report*, vol. 42-221, Jet Propulsion Laboratory, Pasadena, California, pp. 1–23, May 15, 2020. https://ipnpr.jpl.nasa.gov/progress_report/42-221/42-221B.pdf

[2] J. Hamkins, P. Kinman, H. Xie, V. Vilnrotter, and S. Dolinar, "Telemetry Ranging: Concepts," *The Interplanetary Network Progress Report*, vol. 42-203, Jet Propulsion Laboratory, Pasadena, California, pp. 1–20, Nov. 15, 2015. https://ipnpr.jpl.nasa.gov/progress_report/42-203/203C.pdf

[3] M. Stevens, R. Parenti, M. Willis, J. Greco, F. Khatri, B. Robinson, and D. Boroson, "The Lunar Laser Communication Demonstration Time-of-Flight Measurement System: Overview, On-orbit Performance, and Ranging Analysis," in *Free-Space Laser Communication and Atmospheric Propagation XXVIII*, vol. 9739, 2016, p. 973908.

[4] Consultative Committee for Space Data Systems, "Optical Communications Physical Layer," Tech. Rep. CCSDS 141.0-B-1, Aug. 2019.

[5] Consultative Committee for Space Data Systems, "Optical Communications Coding and Synchronization," Tech. Rep. CCSDS 142.0-B-1, Aug. 2019.

[6] J. Hamkins, P. Kinman, H. Xie, V. Vilnrotter, S. Dolinar, N. Adams, E. Sanchez, and W. Millard, "Telemetry Ranging: Laboratory Validation Tests and End-to-End Performance," *The Interplanetary Network Progress Report*, vol. 42-206, Jet Propulsion Laboratory, Pasadena, California, pp. 1–35, Aug. 15, 2016. https://ipnpr.jpl.nasa.gov/progress_report/42-206/206D.pdf

[7] R. Rogalin and M. Srinivasan, "Synchronization for Optical PPM with Inter-Symbol Guard Times," *The Interplanetary Network Progress Report*, vol. 42-209, Jet Propulsion Laboratory, Pasadena, California, pp. 1–19, May 15, 2017. https://ipnpr.jpl.nasa.gov/progress_report/42-209/209C.pdf

[8] S. Stephens and J. Thomas, "Controlled-root formulation for digital phase-locked loops," *IEEE Transactions on Aerospace and Electronic Systems*, vol. 31, no. 1, 1995, pp. 78–95.

[9] R. Rogalin and M. Srinivasan, "Maximum likelihood synchronization for pulse position modulation with inter-symbol guard times," in *2016 IEEE Global Communications Conference (GLOBECOM)*, IEEE, 2016, pp. 1–6.

[10] M. Srinivasan, R. Rogalin, N. Lay, M. Shaw, and A. Tkacenko, "Downlink receiver algorithms for deep space optical communications," in *Free-Space Laser Communication and Atmospheric Propagation XXIX*, vol. 10096, SPIE, 2017, pp. 69–79.

[11] H. Xie, D. Heckman, and J. Breidenthal, "Link Characterization for Deep-Space Optical Communications," *The Interplanetary Network Progress Report*, vol. 42-205, Jet Propulsion Laboratory, Pasadena, California, pp. 1–33, May 15, 2016. https://tmo.jpl.nasa.gov/progress_report/42-205/205D.pdf

APPENDICES

I. Definition of the Range Synchronization Marker

This appendix provides the range synchronization markers obtained while designing the synchronous ranging system proposed in this article. Their values depend on the CSM standardized in [5] as follows:

For the HPE telemetry signaling format, and for $M = 4$, the RSM sequence is

$$[3, 0, 2, 2, 3, 0, 1, 1, 2, 3, 1, 3, 1, 3, 0, 2, 2, 0, 3, 3, 0, 3, 1, 2].$$

For the HPE telemetry signaling format, and for $M = 8$, the RSM sequence is

$$[1, 4, 6, 3, 3, 0, 7, 2, 6, 0, 5, 7, 3, 4, 1, 6].$$

For the HPE telemetry signaling format, and for $M > 8$, the RSM sequence is

$$[10, 9, 10, 10, 8, 7, 1, 4, 5, 6, 15, 13, 0, 7, 6, 8].$$

For the HPE beacon plus accompanying data with LDPC (128, 64), the RSM sequence is 0x928F in binary.

For the HPE beacon plus accompanying data with LDPC (512, 256), the RSM sequence is 0x928F in binary.

For the HPE beacon plus accompanying data with LDPC (2048, 1024), the RSM sequence is 0xDE255C870966485D in binary.

II. Slot Deformation with Spacecraft Dynamics

This appendix derives equations for the time deformation experienced by a slot of duration T_s transmitted from a ground station, coherently turned around by a spacecraft and received by the same ground station. Throughout the derivation it is assumed that the spacecraft range is linear with respect to the ground station and restrict the analysis to a universe in which relativistic effects are neglected.

Figure 19 shows a diagram indicating the different events that occur when sending a single slot from a ground station to a spacecraft. The slot starts departing the ground station at time t_0 and lasts for T_s. It propagates towards the spacecraft at the speed of light c. Therefore, it arrives at the spacecraft when $d(t) = p_u(t)$, where $p_u(t)$ denotes the position of the electromagnetic wavefront as a function of time. This yields

$$t_1 = \frac{1}{1-\gamma}\left(\frac{d_0}{c} + t_0\right) \tag{78}$$

and, consequently,

$$d_1 = c(t_1 - t_0) = \frac{1}{1-\gamma} d(t_0) \approx (1+\gamma) d(t_0), \tag{79}$$

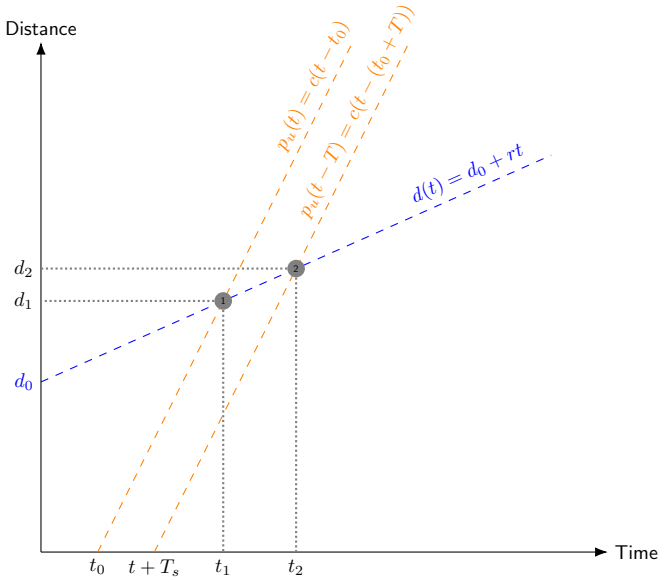

Figure 19. Stretching of the Duration of a PDU Due to Range Rate.

with $\gamma = \frac{r}{c}$. Similarly, the end of the slot starts being propagated at time $t + T_s$. Therefore, its arrival time to the spacecraft will be

$$t_2 = \frac{1}{1-\gamma}\left(\frac{d_0}{c} + t_0 + T_s\right), \tag{80}$$

at which point the distance between the ground station and the spacecraft will be

$$d_2 = \frac{1}{1-\gamma} d(t_0 + T_s) \approx (1+\gamma) d(t_0 + T_s). \tag{81}$$

Therefore, the duration of the slot onboard the spacecraft will be

$$T_s^{sc} = t_2 - t_1 = \frac{1}{1-\gamma} T_s \approx (1+\gamma) T_s. \tag{82}$$

Consider now the operation of a synchronous ranging system, i.e., the downlink signal transmitted by the spacecraft is synchronous to the uplink system. Assume also that the spacecraft introduces a delay τ_{sc} in the synchronicity process. Then the time of departure of the downlink synchronous slot will be

$$t_3 = t_1 + \tau_{sc} \tag{83}$$

and

$$d_3 = d_1 + r\tau_{sc}. \tag{84}$$

Similarly, the end of the downlink slot will start departing at

$$t_4 = t_2 + \tau_{sc}, \tag{85}$$

at which point

$$d_4 = d_2 + r\tau_{sc}. \tag{86}$$

To estimate the time of arrival of the signal, we need to find the trajectory of the RF wavefront as a function of time over the downlink, which we denote $p_d(t)$. In particular, we know that this trajectory will be linear and will satisfy the equation

$$d_3 = -ct_3 + b, \tag{87}$$

where b is an unknown to be adjusted. Basic algebra yields

$$b = \frac{1}{1-\gamma}\left(2d_0 + (c+r)t\right) + (c+r)\tau_{sc}, \tag{88}$$

and thus we can estimate the time of arrival of the downlink slot by solving $p_d(t) = 0$. This results in

$$t_5 = \frac{1}{1-\gamma}\frac{2d_0}{c} + \frac{1+\gamma}{1-\gamma}t + (1+\gamma)\,\tau_{sc}. \tag{89}$$

Repeating the same procedure for the end of the downlink slot yields

$$t_6 = \frac{1}{1-\gamma}\frac{2d_0}{c} + \frac{1+\gamma}{1-\gamma}(t+T_s) + (1+\gamma)\,\tau_{sc}. \tag{90}$$

Finally, we can now calculate different quantities of interest. For example, the duration of a downlink slot as it reaches the ground is

$$T_s^{gs} = t_6 - t_5 = \frac{1+\gamma}{1-\gamma}T_s \approx (1+2\gamma)T_s, \tag{91}$$

where in the second equality we have used the fact that $\frac{1+x}{1-x} \approx 1 + 2x$ for x small. Similarly, the uplink OWLT propagation delay is

$$\tau_u(t) = t_1(t) - t = \frac{1}{1-\gamma}\frac{d(t)}{c} \approx (1+\gamma)\frac{d(t)}{c}, \tag{92}$$

while the downlink OWLT delay is

$$\tau_d(t) = t_5(t) - t_3(t) = \frac{1}{1-\gamma}\frac{d(t)}{c} + \gamma\tau_{sc} \approx (1+\gamma)\frac{d(t)}{c} + \gamma\tau_{sc} \tag{93}$$

and the RTLT delay is

$$\tau_{ud} = t_5(t) - t = \frac{1}{1-\gamma}\frac{2d(t)}{c} + (1+\gamma)\tau_{sc} \approx (1+\gamma)\left[\frac{2d(t)}{c} + \tau_{sc}\right]. \tag{94}$$

III. Ranging Equation Under Linear Motion

This section derives general expressions for the forward and backward RTLT delay under the assumption that the motion between a spacecraft and a ground station is linear. To that end, this article considers the trajectories from Figure 20, in which

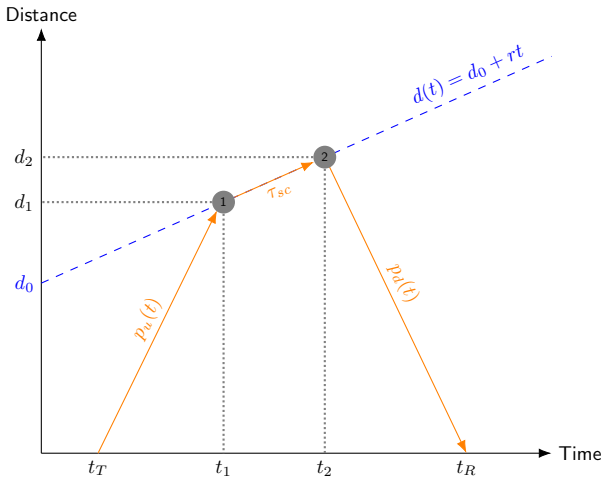

Figure 20. Forward and Backward RTLT Delays.

notation has been kept consistent with the rest of this article. Index 1 denotes the point in time in which the uplink slot starts arriving to the spacecraft. Similarly, index 2 denotes the point in time in which the synchronous downlink slot starts departing from the spacecraft.

From the analysis in Appendix II, we know that

$$t_1(t_T) = \frac{1}{1-\gamma}\left(\frac{d_0}{c} + t_T\right) \tag{95}$$

$$d_1(t_T) = \frac{1}{1-\gamma} d(t_T) \tag{96}$$

$$t_2(t_T) = t_1(t_T) + \tau_{sc} \tag{97}$$

$$d_2(t_T) = d_1(t_T) + r\tau_{sc} \tag{98}$$

$$t_R(t_T) = \frac{1}{1-\gamma}\frac{2d_0}{c} + \frac{1+\gamma}{1-\gamma} t_T + (1+\gamma)\tau_{sc} \tag{99}$$

$$\tau_u(t_T) = \frac{1}{1-\gamma}\frac{d(t_T)}{c} \tag{100}$$

$$\tau_d(t_T) = \tau_u(t_T) + \gamma\tau_{sc} \tag{101}$$

$$\tau_{ud}(t_T) = \frac{1}{1-\gamma}\frac{2d(t_T)}{c} + (1+\gamma)\tau_{sc}. \tag{102}$$

Note that all these functions depend on the departure time of the signal t_T. Therefore, they can be used to evaluate the *forward* uplink and downlink OWLT delays, as well as the *forward* RTLT delay.

To calculate the same functions in the backward direction, one must simply express t_T as a function of t_R and then replace that result in the previous equations. After some

simplification, this yields

$$t_T(t_R) = -\frac{1}{1+\gamma}\frac{2d_0}{c} + \frac{1-\gamma}{1+\gamma}t_R - (1-\gamma)\tau_{sc} \tag{103}$$

$$\tilde{\tau}_u(t_R) = \frac{1}{1+\gamma}\frac{d(t_R)}{c} - \gamma\tau_{sc} \tag{104}$$

$$\tilde{\tau}_d(t_R) = \frac{1}{1+\gamma}\frac{d(t_R)}{c} \tag{105}$$

$$\tilde{\tau}_{ud}(t_R) = \frac{1}{1+\gamma}\frac{2d(t_R)}{c} + (1-\gamma)\tau_{sc}. \tag{106}$$

These expressions can be further simplified using the following Taylor expansion:

$$\frac{1}{1\mp x} \approx 1 \pm x \tag{107}$$

$$\frac{1\pm x}{1\mp x} \approx 1 \pm 2x, \tag{108}$$

which results in

$$\tau_{ud}(t_T) \approx (1+\gamma)\left[\frac{2d(t_T)}{c} + \tau_{sc}\right] \tag{109}$$

$$\tilde{\tau}_{ud}(t_R) \approx (1-\gamma)\left[\frac{2d(t_R)}{c} + \tau_{sc}\right]. \tag{110}$$

Also, observe that the following relationships hold as expected:

$$\tau_{ud}(t_T) = \tau_u(t_T) + \tau_d(t_T) + \tau_{sc} \tag{111}$$

$$\tilde{\tau}_{ud}(t_R) = \tilde{\tau}_u(t_R) + \tilde{\tau}_d(t_R) + \tau_{sc}. \tag{112}$$

IV. Range-Rate Post-Compensation

This appendix provides the necessary expressions to recover the PPM symbol timing at the receiver when range-rate post-compensation is applied to the received signal. This appendix also shows that post-compensation allows the receiver to increase the integration time used for phase estimation, which in turn permits operation at worse signal and noise conditions.

A. Symbol Timing with Range-Rate Post-Compensation

To start, consider an optical link between a transmitter and a receiver using PPM modulation. Let t_1 denote the departure time of an arbitrary signal photon from the transmitter, and let t_2 denote its reception time at the receiver. Then, in general, we know that

$$t_2 = t_1 + \tau(t_1), \tag{113}$$

where $\tau(t_1)$ denotes the forward OWLT. Furthermore, if the distance between transmitter and receiver is linear, then

$$\tau(t) = \frac{1}{1-\gamma}\frac{d_0 + rt}{c} \approx (1+\gamma)(\tau_0 + \gamma t) \approx \tau_0 + \gamma t, \tag{114}$$

where $\tau_0 = d_0/c$ and we have used the fact that $1 + \gamma \approx 1$ and $\gamma^2 \ll \gamma$.

Assume that the receiver is based on a photon-counting device as shown in Figure 13 so that discrete time tags of all detected photons are available for processing. Further, assume that the receiver's trajectory during the link operation can be predicted, and thus an estimate of the range rate can be precomputed and provided to the receiver as a priori information. Let $\hat{\gamma}$ denote this estimate.[16]

To perform range-rate post-compensation, the receiver takes the incoming time tags and applies the following transformation:

$$t_2' = \frac{t_2}{1+\hat{\gamma}} \approx (1-\hat{\gamma})t_2. \tag{115}$$

Consequently,

$$t_2' \approx (1-\hat{\gamma})(t_1 + \tau(t_1)) = t_1 + \underbrace{(1-\hat{\gamma})\tau(t_1) - \hat{\gamma}t_1}_{\tau'(t_1)}, \tag{116}$$

where $\tau'(t_1)$ denotes the *apparent* OWLT that the receiver signal-processing chain will experience after range-rate post-compensation is applied. Moreover, assuming linear relative motion between transmitter and receiver, we have that

$$\begin{aligned} \tau'(t_1) =& (1-\hat{\gamma})(\tau_0 + \gamma t_1) - \hat{\gamma}t_1 \\ =& \left[(1-\hat{\gamma})\gamma - \hat{\gamma}\right] t_1 + (1-\hat{\gamma})\tau_0 \\ \approx& (\gamma - \hat{\gamma})t_1 + \tau_0. \end{aligned} \tag{117}$$

In the last step, we have used that $1 - \hat{\gamma} \approx 1$ and $\gamma\hat{\gamma} \ll \hat{\gamma}$. In other words, we have shown that by applying the transformation of Equation (115), the receiver operates with observables that only contain the residual range rate $\epsilon_\gamma = \gamma - \hat{\gamma}$.

In general, once the slot synchronizer has locked, an estimate of the time of arrival of the i-th PPM symbol can be recovered as follows:[17]

$$t_{PPM_i} = t_i + \varphi(t_i), \tag{118}$$

where $t_i = (M+P)T_s i$ denotes the time of departure of the i-th PPM symbol. However, because of range-rate post-compensation, the slot synchronizer is tracking t_i' and $\varphi'(t)$ instead of t_i and $\varphi(t)$. Consequently, to recover the actual symbol clock from the PLL observables, we use

$$t_{PPM_i} = (1+\hat{\gamma})\left[t_i' + \varphi'(t_i')\right]. \tag{119}$$

B. Integration Time with Range-Rate Post-Compensation

As noted in Section III.B, the bias of the one-shot phase estimator depends on integration time used to calculate the phase estimate. This happens because the

---

[16] For consistency's sake, $\hat{\gamma}$ is an estimate of $\gamma = \frac{r}{c}$.

[17] This expression assumes that the transmitter does not apply range-rate pre-compensation.

one-shot estimator produces a single-phase estimate using samples captured over a period of time during which the received phase was actually constantly changing. Thus, if the integration period is set to a large enough value, the ML estimator will fail to produce a phase estimate altogether.

Let t_1 be the start of the integration period and $t_2 = t_1 + T_{int}$ be its end. Then the received phase at the start and end of the integration period will be

$$\varphi(t_1) = \frac{\tau(t_1)}{T} \approx \frac{\tau_0 + \gamma t_1}{T} \tag{120}$$

$$\varphi(t_2) = \frac{\tau(t_2)}{T} \approx \frac{\tau_0 + \gamma(t_1 + T_{int})}{T}. \tag{121}$$

Consequently, the phase difference between the start and end of the integration period is

$$\Delta\varphi = |\varphi(t_2) - \varphi(t_1)| = \frac{|\gamma| T_{int}}{T} = |\gamma| N_{int} \tag{122}$$

with N_{int} equal to the number of PPM symbols used in the integration period.

Consider now the case where the received time tags are range-rate post-compensated. Then, by virtue of the analysis in Section IV.A, the same reasoning is valid, except that instead of the full range rate γ, the slot synchronizer will only experience the residual range rate ϵ_γ. Therefore, with range-rate post-compensation, the phase difference between the start and end of an integration period is

$$\Delta\varphi' = |\varphi'(t_2) - \varphi'(t_1)| = \frac{|\epsilon_\gamma| T_{int}}{(M+P)T_s} = |\epsilon_\gamma| N_{int}. \tag{123}$$

To achieve the same performance with and without range-rate post-compensation, the phase error introduced in any given integration period must be the same. Hence,

$$|\gamma| N_{int} = |\epsilon_\gamma| N'_{int}, \tag{124}$$

which yields

$$N'_{int} = \left|\frac{\gamma}{\epsilon_\gamma}\right| N_{int} = \frac{1}{1 - \left|\frac{\hat{\gamma}}{\gamma}\right|} N_{int}. \tag{125}$$

Note that $|\epsilon_\gamma/\gamma|$ is the relative error in the range-rate prediction provided to the receiver. Therefore, as expected, if you had a perfect prediction $\hat{\gamma} = \gamma$ and $|\epsilon_\gamma/\gamma| \to \infty$, indicating that all the receiver dynamics have been post-compensated, and thus the user is free to select an infinitely large integration period. From a practical standpoint, this indicates that having good predicts of the spacecraft dynamics not only facilitates the job of the receiver electronics, but it also allows the system to operate at lower signal and/or higher noise conditions by allowing the user to configure longer integration times for clock recovery.